Characterization of polymers and contacts in polymer light emitting diodes

Kristensen, Peter Kjær

Publication date:
2008

Document Version
Publisher's PDF, also known as Version of record

Peter Kjær Kristensen

Characterization of polymers and contacts in polymer light emitting diodes

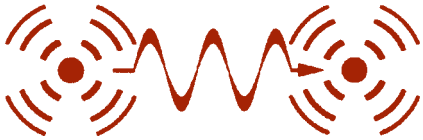

Department of Physics and Nanotechnology
Aalborg University, Denmark

Characterization of polymers and contacts in polymer light emitting diodes

Karakterisering af polymerer og kontakter i polymere lys emitterende dioder

Published and distributed by
Department of Physics and Nanotechnology, Aalborg University
Skjernvej 4a, DK–9220 Aalborg Øst.
Phone +45 99 40 80 80. Fax +45 98 15 65 02.

Typeset in LaTeX2$_\varepsilon$ by the author.

Printed in Denmark by Centertrykkeriet, Aalborg University.

ISBN 87-89195-26-4

Preface

This PhD thesis is based on the results obtained during my PhD studies at the Department of Physics and Nanotechnology, Aalborg University, Denmark and at Optics and Plasma Research Department, Risø National Laboratory, Denmark under skilled supervision of Dr. Thomas Garm Pedersen and Dr. Per Michael Johansen. The thesis has been submitted to the Faculty of Engineering and Science at Aalborg University.

Outline

Part I is an introduction to organic molecules in general and conjugated polymers in particular. A description of the source of the semiconducting nature in simple conjugated polymers is included. Furthermore, an ab initio approach for modeling of conjugated polymers is introduced and applied to conjugated porphyrin polymers and the results of the study have been published[1]. Finally, methods for producing thin polymer films to be used in devices based on conjugated polymers and some basic concepts for light emission in conjugated polymers, are explained.

Part II is based on the scientific papers [2, 3], and includes a description of the polymers investigated and the results of these investigations. The primary focus is put on the emissive properties of the polymers, both in photo- and in electroluminescence, and in cases where these differ, the difference has been explained. The conjugated polymers have light emission spanning the entire visible range. Finally intermolecular energy transfer from a blue emitting polymer to a red emitting Eu complex doped into the polymer has been described. The purpose of the doping is to achieve red emission suitable for red emission in displays based on conjugated polymers.

Part III is based on the scientific paper [4], and describes techniques for characterization of the contact materials used in polymer light emitting diodes.

The contact materials have great effect on the device operation and efficiency and therefore a thorough characterization is important.

Acknowledgements

I am grateful to Donghong Yu and Kaizheng Zhu from the Department of Life Sciences, Section for Chemistry at Aalborg University for producing such nice polymers for me to investigate and characterize. I also would like to thank all my colleagues at the Department of Physics and Nanotechnology for all your help during my studies. Special thanks goes to Kim H. Jensen for helping me solving all the practical problems in fabrication of polymer light emitting diodes and Jens Rafaelsen and Kjeld Pedersen for helping me build the setup for the EFISH measurements.
Financial support from STVF grant #26-02-0227 is gratefully acknowledged.

Aalborg, Denmark, September 2008 **Peter Kjær Kristensen**

Contents

Part I

Organic Light Emitting Diodes

Chapter 1

Organic Molecules

Organic materials have been known to be electroluminescent since 1963, when Pope *et al.*[5] demonstrated electroluminescence (EL) in anthracene crystals. The chemical structure of anthracene is illustrated in Fig. 1.1. In the work by Pope *et al.* the anthracene crystal was sandwiched in a structure between two identical electrodes. The use of different materials for cathode and anode has since been applied to anthracene crystals with a semitransparent anode and a solid or liquid cathode. The anthracene crystal is a typical example of the polyaromatic branch of the low molecularweight organic materials used for EL. The polyaromatic branch also include derivatives of anthracenes, perylenes and stilbenes. In the work by Pope *et al.* the crystals are grown either from solution or prepared by sublimation giving crystals thickness of $10\mu m$ and $20\mu m$. Because the crystals are relatively thick, the photoluminescence spectrum can be quite different from the electroluminescence spectrum. The primary source of the difference is re-absorption of the light emitted, which occurs because the crystals are thick. Because PL and EL do not have the same emission centers the effect of re-absorption will be different in the two cases.

In the following decades there were relatively low interest in EL from organic materials until 1987, when Tang and VanSlyke[6] demonstrated EL from the

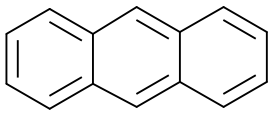

Fig. 1.1: The chemical structure of anthracene.

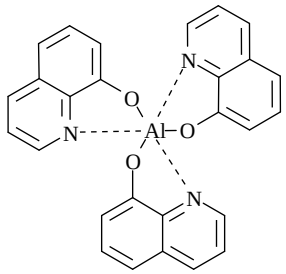

Fig. 1.2: The chemical structure of 8-hydroxyquinoline aluminum.

fluorescent metal-chelate complex, 8-hydroxyquinoline aluminum (Alq_3), see Fig. 1.2 for the chemical structure. Metal-chelates are metal ions with ligands attached to form a metal complex. In devices the complexes form thin organic films with thickness ranging between $50nm$ and $10\mu m$ and with electrodes on either side. The devices can be made both as single layer devices with only the emissive layer between the electrodes and as multilayer devices, where the additional layer(s) are hole and/or electron transport layers. Tang and VanSlyke used a two layer device with aromatic diamine as hole transport layer and Alq_3 as emitting layer, which has peak emission at $528nm$ and FWHM of $100nm$. These were sandwiched between the hole injecting electrode, indium tin oxide (ITO), and the electron injecting electrode, a silver-magnesium alloy. Both organic layers and the metal alloy were deposited onto an ITO coated glass substrate by thermal evaporation. Similar device structures has been used extensively since, that is an emitting layer sandwiched between a hole injecting electrode with high workfunction and an electron injecting electrode with low workfunction, resulting in a diode as opposed to the device used by Pope *et al.* which used two identical electrodes. Using different electrodes for hole and electron injection increases the efficiency of charge injection and overall device efficiency. In the device by Tang and VanSlyke the magnesium in the silver-magnesium alloy acts as the low workfunction electron injector, whereas the silver protect against oxidation and improve the sticking abilities of Mg. As hole injecting electrode ITO has been used extensively because it has a high workfunction and is transparent in the visible range, allowing light from the emitting layer to escape. As electron injecting electrode a variety of metals and alloys have been used. Because the diamine has low electron mobility and because Alq_3 is an efficient electron transport layer, exciton formation and decay are restricted to the interface between diamine and Alq_3.

A major advancement with Alq_3 compared to anthracene crystals, was the lowering of the drive voltage. In anthracene crystals EL were first observed above 400V, whereas EL from Alq_3 was measurable with a drive voltage as low

as 2.5V. The initial device fabricated by Tang and VanSlyke had an efficiency of ∼1%. This was later improved by Tang *et al.*[7] by doping the light emitting Alq_3 with highly fluorescent molecules to give an efficiency of ∼2.5%. Doping of the luminescent material has also been done in anthracene. The doping of Alq_3 also enabled Tang *et al.* to tune the emission from blue-green to orange-red depending of the dopant. The increase in device efficiency is due to the dopants high fluorescent efficiency ($> 50\%$) compared to the relatively low efficiency of Alq_3 of 8%. However, Alq_3 is still needed because it is an efficient electron transport layer. The Alq_3 is also important to the luminescent properties of the blend because the pure dopants have low fluorescent efficiency in solid state due to concentration quenching. In the devices made by Tang *et al.* the efficiency peaks when the dopants were blend in Alq_3 in $0.5 - 1\%$ concentrations. The dopants are either excited directly or through energy transfer from the Alq_3 host.

Other metal-chelates than Alq_3 have been used in EL devices. To achieve efficient light emission from these devices, the metal-chelate has to have high fluorescence efficiency also in solid state. Fluorescent metal-chelates are usually molecules with a central metal ion from group II (e.g. Be^{2+} and Zn^{2+}) or III (e.g. Al^{3+}) in the periodic chart. The 8-hydroxyquinoline-ligands used in Alq_3 have also been used with other metals both from group II (Pt and Pb) and group III (Bi, Rh, and Ir) to give fluorescence and phosphorescence[8]. The molecules with heavy atoms (Pt, Pb, Bi, and Ir) at the center exhibit phosphorescence, whereas the lighter atoms (Al and Rh) exhibit fluorescence. To achieve efficient fluorescence the following conditions should be met:

1. The metal ion must not be paramagnetic, because a paramagnetic metal ion will lead to intersystem crossing from singlet to triplet state.

2. The metal ion must not be heavy, since this also leads to intersystem crossing as demonstrated by Ballardini *et al.*[8]

Besides affecting the fluorescence/phosphorescence probability the choice of metal ion also determine the position of the emission peaks, with green emission from metal-chelates containing Al(528nm), Pb(550nm), and Bi(540nm) and red emission from metal-chelates containing Rh(622nm), Ir(660nm), and Pt(655nm). In the case of Alq_3, the emission properties can also be controlled by modifying the chemical structure of the ligand, because the 3 lowest electronic transitions responsible for the fluorescence are located on the ligand whereas higher electronic transitions are delocalized to neighboring ligands. The changes in emission depends on where in the ligand the modifications are made and which modification are made, see Fig. 1.3. Modifications to the phenoxide (positions 5 and 7 in Fig 1.3) changes the level of the highest occupied molecular orbital (HOMO), whereas making modifications to the pyridyl (positions 2 and 4 in Fig 1.3) changes the lowest unoccupied molecular orbital (LUMO). Adding an electron-withdrawing substitute to the phenoxide or pyridyl, lowers the positions of the HOMO or

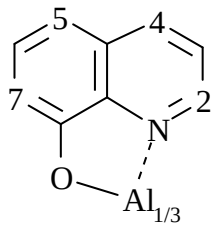

Fig. 1.3: The chemical structure of the 8-hydroxyquinoline ligand.

LUMO, respectively, whereas adding an electron-donating substitute raises the HOMO or LUMO. Lowering the HOMO or raising the LUMO would increase the energy gap and thus blue-shift the emission while raising the HOMO or lowering the LUMO would decrease the energy gap and red-shift the emission. The method has been demonstrated by adding the electron-withdrawing N to position 4 to give AlX_3[9] and to position 5 to give $Al(NQ)_3$[10]. As predicted the AlX_3 is red-shifted compared to Alq_3 about 50nm to 580nm whereas $Al(NQ)_3$ is blue-shifted 90nm to 440nm. Adding electron-donating substitutes have also been investigated and it has been found that the predictions also holds in this case[11].

Chapter 2

Conjugated Polymers

Conjugated polymers (CP) are polymers with dimerized pattern of alternating double and single bonds. In CP the $2s$, $2p_x$, and $2p_y$ atomic orbitals in carbon forms the skeleton of the polymer. These orbitals, named sp^2 which overlap when two carbon atoms are brought together form a strong covalent bond, the σ-bond. The sp^2 orbitals are highly localized whereas the p_z forms delocalized orbitals or π-orbitals. The conjugated polymers are semiconducting due the to the delocalized π-electrons. These electrons form bonding (π) and antibonding (π^*) orbitals. With one electron per site the lower half of the orbitals are occupied (bonding orbitals) and the upper half are unoccupied (antibonding) resulting in valence and conduction wavefunctions. As the name implies the bonding orbitals also contribute to the bonding of the molecule. Therefore the configuration of the molecule is dependent on whether the molecule is excited, because the carbon to carbon bond lengths depend on this. This dependence is seen experimentally through the coupling of electronic and vibrational transitions.

Polymers are often modeled as infinite chains which is obviously not the case for real polymers. Instead samples have a distribution of molecular weights. A sample is therefore composed of chains with varying lengths. Furthermore the real polymers have defects along the polymer chain which breaks the conjugation. It is convenient to define the conjugation length as the average distance between these defects.

2.1 Polyacetylene - A Case Example

A prototype of CP is the polyacetylene with a C_2H_2-unit cell. Polyacetylene comes in two configurations or isomeric forms depicted in Fig. 2.1, with trans-polyacetylene on the left and cis-polyacetylene on the right, the former being thermodynamically stable[12]. Trans-polyacetylene can be treated with a tight-binding model of the π-electrons. The polymer is modelled as a chain with two

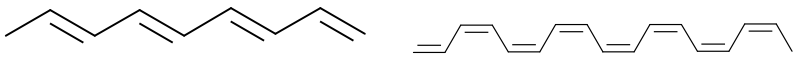

Fig. 2.1: Left: trans-transoidal, or trans-polyacetylene. Right: cis-transoidal, or cis-polyacetylene.

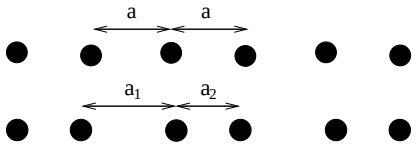

Fig. 2.2: Upper: The non-dimerized one-dimensional polyacetylene chain. Lower: The dimerized one-dimensional polyacetylene chain.

atoms per unit cell, the two carbon atoms, and one orbital per atom, the π-orbital. Two situations will be considered, first the situation with the same bond distance between all carbon atoms, the non dimerized situation, and second the situation with alternating bond distances, the dimerized situation, depicted as the upper and lower part in Fig. 2.2, respectively. This gives us the following Bloch sums for the two orbitals in the non-dimerized case:

$$\begin{aligned} |a1(\boldsymbol{r})\rangle &= \frac{1}{\sqrt{N}}\sum_{n=1}^{N}\exp(ikn2a)|\phi(\boldsymbol{r}-2na\hat{\boldsymbol{z}})\rangle, \\ |a2(\boldsymbol{r})\rangle &= \frac{1}{\sqrt{N}}\sum_{n=1}^{N}\exp(ik(2n+1)a)|\phi(\boldsymbol{r}-(2n+1)a\hat{\boldsymbol{z}})\rangle, \end{aligned}$$

with N being the number of unitcells, a the bond distance between to carbon atoms, and $\phi(\boldsymbol{r})$ the atomic orbital. The general wavefunction $|\Psi(\boldsymbol{r})\rangle$ is a linear combination of the two Bloch sums:

$$|\Psi(\boldsymbol{r})\rangle = c_1(k)|a1(\boldsymbol{r})\rangle + c_2(k)|a2(\boldsymbol{r})\rangle.$$

The generalized eigenvalue problem can be calculated using the energy and overlap integrals:

$$H_{\alpha\beta} = \langle a\alpha(\boldsymbol{r})|H|a\beta(\boldsymbol{r})\rangle, \tag{2.1}$$
$$S_{\alpha\beta} = \langle a\alpha(\boldsymbol{r})|a\beta(\boldsymbol{r})\rangle, \tag{2.2}$$

and solving:

$$\left(\overleftrightarrow{\mathbf{H}} - E(k)\overleftrightarrow{\mathbf{S}}\right)\cdot\boldsymbol{c}(k) = 0, \tag{2.3}$$

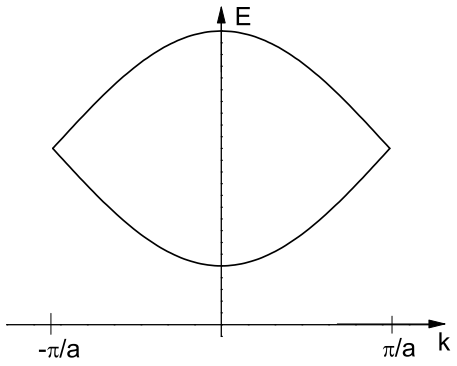

Fig. 2.3: Band structure for π-electron in non-dimerized polyacetylene, calculated from (2.6).

with $\boldsymbol{c}(k) = (c_1(k), c_2(k))$. Calculating the energy integrals (2.1) with nearest neighbors contributions and the overlap integrals (2.2) with only on-site contributions, the eigenvalue problem (2.3) is:

$$\left(\begin{pmatrix} E_{p1} & 2E_{p2}\cos(ka) \\ 2E_{p2}\cos(ka) & E_{p1} \end{pmatrix} - E(k) \begin{pmatrix} 1 & 0 \\ 0 & 1 \end{pmatrix} \right) \cdot \begin{pmatrix} c_1(k) \\ c_2(k) \end{pmatrix} = 0, \tag{2.4}$$

with $E_{p1} = H_{11} = H_{22}$ and $E_{p2} = H_{12} = H_{21}$. The only non-trivial solution to (2.4) is:

$$\begin{vmatrix} E_{p1} - E(k) & 2E_{p2}\cos(ka) \\ 2E_{p2}\cos(ka) & E_{p2} - E(k) \end{vmatrix} = 0. \tag{2.5}$$

The two solutions to (2.5):

$$E(k) = E_{p1} \pm 2E_{p2}\cos(ka), \tag{2.6}$$

are depicted in Fig. 2.3. The Bloch sums in the dimerized case are

$$\begin{aligned} |b1(\boldsymbol{r})\rangle &= \frac{1}{\sqrt{N}} \sum_{n=1}^{N} \exp(ik(n(a_1 + a_2) + a_1)) \\ |b2(\boldsymbol{r})\rangle &= \frac{1}{\sqrt{N}} \sum_{n=1}^{N} \exp(ik(n(a_1 + a_2) - a_2)), \end{aligned}$$

where a_1 and a_2 are as defined in Fig. 2.2. The non-trivial solution to the eigenvalue problem is in this case:

$$\begin{vmatrix} E_{p1} - E(k) & \beta_1 \exp(ika_1) + \beta_2 \exp(-ika_2) \\ \beta_1 \exp(-ika_1) + \beta_2 \exp(ika_2) & E_{p1} - E(k) \end{vmatrix} = 0, \tag{2.7}$$

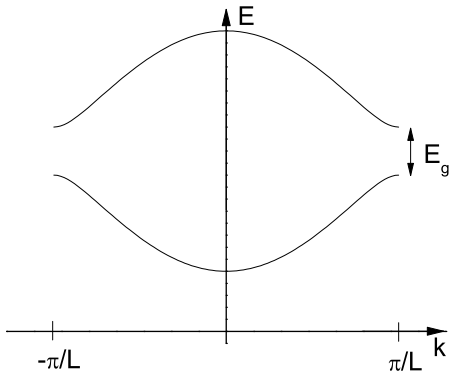

Fig. 2.4: Band structure for π-electron in dimerized polyacetylene, calculated from (2.8).

with the energy integrals β_1 and β_2 defined as:

$$\begin{aligned} \beta_1 &= \langle \phi(\boldsymbol{r})|H|\phi(\boldsymbol{r} \pm a_1\hat{\boldsymbol{z}})\rangle, \\ \beta_2 &= \langle \phi(\boldsymbol{r})|H|\phi(\boldsymbol{r} \pm a_2\hat{\boldsymbol{z}})\rangle. \end{aligned}$$

The two solutions to (2.7) are :

$$E(k) = E_{p1} \pm \sqrt{\beta_1^2 + \beta_2^2 + 2\beta_1\beta_2 \cos(k(a_1 + a_2))}, \tag{2.8}$$

and the resulting band structure is shown in Fig. 2.4. From Fig. 2.3 and Fig. 2.4 it is apparent that the non-dimerized chain has no bandgap as opposed to the dimerized chain, which has a bandgap at $\frac{\pi}{L}$, where $L = a_1 + a_2$. In other words, dimerized polyacetylene is a semiconductor. The size of the bandgap is $E_g = 2|\beta_1 - \beta_2|$.

2.2 Density Functional-based Tight-Binding

To give a more complete description of polymers a more sophisticated model has to be applied. One such model could be the Density Functional-based Tight-Binding (DFTB) approach developed by Porezag *et al.* in 1995[13]. The DFTB approach is an extension to the tight-binding model introduced in Sec. 2.1. The extension includes calculating the two center integrals (2.1) and (2.2) as a function of distance for a number of combinations of atoms using Density Functional Theory (DFT). The two center repulsive potential as a function of distance was also extracted for a number of atom combinations from DFT calculations. From these extensions it is possible to calculate the total energy composed of the electron band structure energy and the repulsive potentials. By minimizing the total

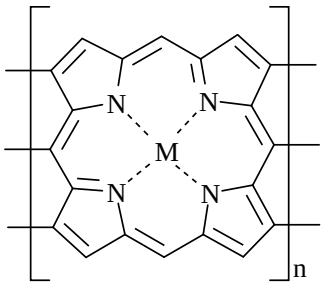

Fig. 2.5: The chemical structure of metalloporphyrin polymers.

energy calculated using DFTB, the optimized configurations, optical gaps and phonon energies of polymers can be found[14].

The DFTB approach has been applied to conjugated porphyrin polymers, and the results where published in Ref. [1]. The chemical structure of a metalloporphyrin polymer, i.e. a porphyrin polymer with a metal ion at the center, is illustrated in Fig. 2.5. The main purpose of this study was to determine the exciton binding energy of the conjugated porphyrin polymers, which are known to have absorption bands at energies as low $0.43eV$[15] making them candidates for either organic infrared LEDs or infrared solar cells depending on the exciton binding energy. A high exciton binding energy is desirable in LEDs since this will increase the probability of radiative exciton decay, whereas a small binding energy will increase the probability of electron-hole separation in solar cells. The study showed that porphyrin polymers have a small exciton binding energy $< 0.2eV$ and the polymers were suggested as candidates for solar cells absorbing in the infrared part of the spectrum. Furthermore, it was found that introducing a metal ion at the center of the porphyrin monomer instead of the two hydrogen atoms, significantly changed the absorption and exciton energies whereas the choice of metal ion was less significant. The significant change upon introduction of the metal ion was attributed low lying unoccupied p_z-orbitals which couple to the unoccupied π^*-bands in the porphyrin polymer.

2.3 Synthesized Conjugated Polymers

An example of a CP will now be considered. More specifically PPV, which was the CP first to demonstrate to demonstrate EL[16]. In CP a planer structure is often favorable because this leads to the strongest bonding. This is true for polyacetylene and it has been experimentally demonstrated that PPV has a dihedral angle as small as $7^o \pm 6^o$[17]. The planer structure means CP tend to be rigid

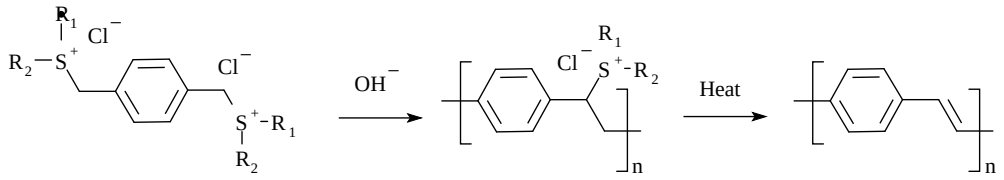

Fig. 2.6: The precursor route to PPV. The precursor polymer is converted to the final polymer by heating.

and insoluble. This is indeed the case for PPV and the resulting polymer from direct polymerization of the monomer will be insoluble.

Furthermore this CP demonstrates the two different methods of forming films needed in EL devices. The first of these two methods are the precursor where the film is formed from a precursor polymer which is soluble. Through further processing steps the precursor polymer is then transformed to the final polymer. In the second method the polymer is made soluble. Once the polymer is soluble it is desolved in a solution and spincoated.

2.3.1 Precursor Route

The processing steps to convert the precursor polymer to the final polymer could for instance be heating. The sulfonium precursor route to PPV was developed by Wessling and Zimmerman in 1968[18]. The desolvable precursor polymer is prepared from a base-induced polymerization of a p-xylylenebis(alkylsufonium) salt as depicted in Fig. 2.6. The precursor polymer is converted to the final polymer by heating. A different precursor route was introduced by Burroughes *et al.* in 1990[16]. This route is illustrated in Fig. 2.7. In this precursor route α, α'-dichloro-p-xylene was used to form a sulphonium salt, which was polymerized to the desolvable precursor polymer. The transformation to the final polymer was performed by heating in vacuum. The precursor route introduced by Burroughes *et al.* was a modification of a route, which has been demonstrated to give higher molecular weight[19] than the original route introduced by Wessling and Zimmerman. The higher molecular weight also leads to longer conjugation length. One advantage of the precursor routes is that the films formed are insoluble, which can be convenient if further processed is performed to the films.

2.3.2 Solution Processible

In solution processible polymers modifications are made to make the final polymer soluble rather the the precursor polymer. Therefore the thermal conversion necessary in the precursor routes is avoided. Usually PPV is made soluble by attaching side groups to positions 2 and 5 on the phenyl ring, see Fig. 2.8. The

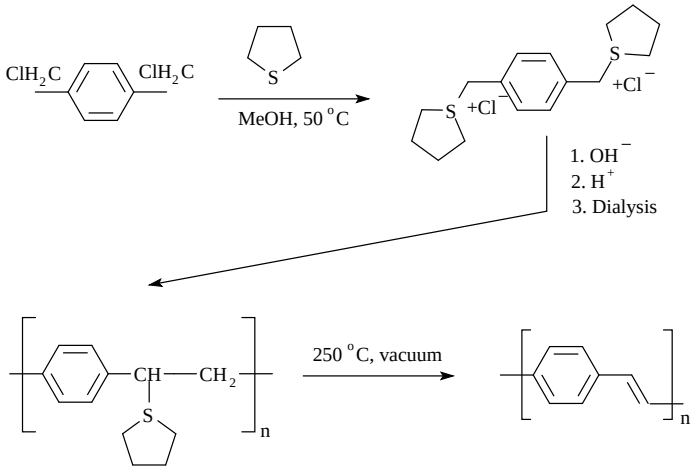

Fig. 2.7: The precursor route developed by Burroughes *et al.*[16].

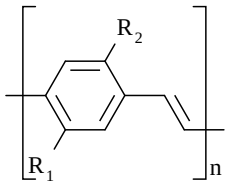

Fig. 2.8: In order to make PPV soluble side groups are attached to position 2 and 5 on the phenyl ring.

side chains keep the polymer backbones apart making the polymer more soluble. The attached side chains are often alkoxy groups, as it was the case for the first soluble PPV, poly(2,5-dihexyloxy-p-phenylenevinylene)[20]. The structure is depicted in Fig. 2.9. Alkoxy groups are composed of oxygen and alkyl, where alkyl are radicals with the general formula C_nH_{2n+1}. The alkoxy-PPV can be prepared either by the Wessling and Zimmerman precursor route or by a dehalogenation reaction - condensation polymerization. The soluble PPV was first reported in 1989 before Burroughes *et al.* reported EL from precursor PPV in september 1990. Only a few months later in february 1991 Braun and Heeger reported EL from the soluble poly(2-methoxy-5(2'-ethyl-hexyloxy)-p-phenylenevinylene), MEH-PPV depicted in Fig. 2.10[21]. In general, attaching asymmetric side groups makes the polymers more soluble, as it is the case for the branched alkoxy group in MEH-PPV. Besides making the polymer more soluble the alkoxy side

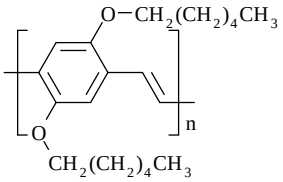

Fig. 2.9: The chemical structure of poly(2,5-dihexyloxy-p-phenylenevinylene)

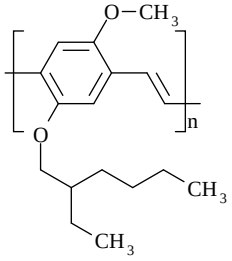

Fig. 2.10: The chemical structure of poly(2-methoxy-5(2'-ethyl-hexyloxy)-p-phenylenevinylene), MEH-PPV

groups bound to the phenyl ring also changes the luminescence properties of PPV. The precursor PPV investigated by Burroughes *et al.* showed a peak at 2.2eV (564nm) whereas MEH-PPV has a peak at 2.1eV(590nm), that is the alkoxy side groups lead to red-shift of the light emission.

2.4 Excitons

Light emitting diodes (LEDs) operate through radiative exciton decay to produce light. Electrons and holes are injected into the polymer and they capture each other to form a neutral bound state, the exciton. The capture is of Langevin type, that is a random motion within an attractive potential with a capture radius r_c of:

$$r_c = \frac{e^2}{4\pi\epsilon k_B T},$$

where e is the elementary charge, ϵ is the permittivity of the polymer, k_B is the Boltzmann constant, and T is the temperature. The exciton can be localized around one molecule, in which case it is termed a Frenkel exciton after J. Frenkel. It can also be delocalized over several molecules, termed the Mott-Wannier exciton, named after Sir Nevill Francis Mott and Gregory Wannier. The exciton is

Fig. 2.11: A trans-polyacetylene chain containing a soliton.

also classified according to the spin. Because it is composed of two spin $\frac{1}{2}$ charges the total spin of the exciton is either $S = 0$, the singlet, or $S = 1$, the triplet. The Pauli exclusion principle dictates that only the singlet results in light emission. Triplet to singlet conversion is possible. The conversion requires energy, the exchange energy, which is the energy difference between the triplet and the singlet state. The efficiency of the light emission from exciton decay η_{exi} can be defined as:

$$\eta_{exi} = \eta_{es}\eta_{sr}, \tag{2.9}$$

where η_{es} is the fraction of excitons formed which are singlets and η_{sr} is the fraction of singlets which decay radiatively. Simple spin statistics predicts that the triplet to singlet ratio is 3:1, that is the maximum efficiency is 25%. Non-radiative singlet decay also occurs in all CP. Trans-polyacetylene shows no luminescence indicating all singlet decay is non-radiative whereas cis-polyacetylene does show luminescence[22]. The absence of luminescence in trans-polyacetylene is assumed to due to presence of solitons in the polymer chain. The solitons makes the polymer photoconductive and non-luminescent. A soliton, see Fig. 2.11, is a shift in the alternation of the double and single bonds. Solitons are present in trans-polyacetylene due to the degenerate ground state in the polymer. The ground state in trans-polyacetylene is degenerate because the single and double bonds are interchangeable, see Fig. 2.1.

Absorption and emission of light in a molecule is per definition a Frenkel exciton. However, once molecules form a solid, the intermolecular Mott-Wannier exciton is to be considered. The energy levels are given by a modified Rydberg equation:

$$E_n = E_g - \frac{\mu e^4}{(4\pi\epsilon_0\epsilon_r\hbar)^2}\frac{1}{n^2},$$

with μ being the reduced effective mass defined by:

$$\frac{1}{\mu} = \frac{1}{m_e} + \frac{1}{m_h}$$

m_e and m_h are the effective masses of the electron and hole respectively, and ϵ_r being the relative permittivity. From these considerations the effective Bohr

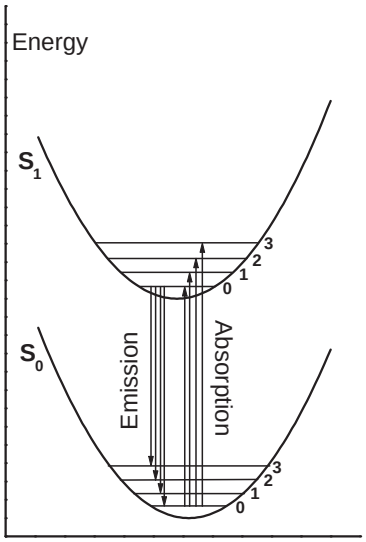

Fig. 2.12: Energy level diagram illustrating electron-phonon coupled transitions.

radius of the exciton can be estimated to:

$$a_b = \frac{4\pi\epsilon_0\epsilon_r\hbar^2}{\mu e^2}.$$

For excitons to be classified as Mott-Wannier, the Bohr radius have to be substantially larger than the distance between individual molecules. That is, the reduced effective mass has to be small and the relative permittivity has to be large. Gommes da Costa and Conwell have considered a PPV and found that it is anisotropic with different reduced effective masses and relative permittivities along the chain compared to perpendicular to the chain, resulting in an exciton with a size of $2nm$ along the chain and $0.4nm$ perpendicular to the chain[23]. Gommes da Costa and Conwell also found the binding energy of the exciton to be $0.4eV$. From these considerations it can be concluded that the exciton in PPV is confined to a single molecule and it can therefore be classified as a Frenkel exciton. The confinement of the exciton to a single molecule results in coupling between electron and lattice, which is observed in the coupling between the electronic and vibrational transitions mentioned earlier. The energy levels involved in electron-phonon coupled transitions are illustrated in Fig. 2.12. In Fig. 2.12 S_0 and S_1 on the left indicate the electronic transitions whereas 0, 1, 2, and 3 on the right indicate how many phonons are involved in the transitions. On other words, the energy difference between 0 and 2 are double the energy difference between 0 and 1 because the former involves two phonons identical to the one in the latter. This is the case for both S_0- and S_1- levels. The probability of a

transition is given by:

$$P = \frac{\exp(S)S^n}{n!}, \tag{2.10}$$

where S is the Huang-Rhys parameter. If a molecule is vibrationally excited it will relax to the unexcited state very fast ($\sim 10^{-13}s$) and as a consequence of the fast vibrational relaxation transitions will always occur from the vibrational ground state. That is, in absorption the transition will always be $S_{0,0} \rightarrow S_{1,n}$, where $S_{0,0}$ is the vibrational ground state of S_0 and $S_{1,n}$ is the S_1 excited with n phonons and $n = 0, 1, 2, 3, \cdots$. In emission, on the other hand, it is the electronically excited state which is vibrationally relaxed and emission transition will consequently always be $S_{1,0} \rightarrow S_{0,n}$. Due to relaxation of the molecule in the excited state the $S_{0,0} \leftrightarrow S_{1,0}$ transition will be red shifted in emission compared to absorption. This shift is termed Stokes shift after George G. Stokes.

It has been demonstrated that the Coulomb interactions are of great importance for understanding the spectroscopy of PPV in the spectral range of the lowest allowed electronic transitions[24]. In the modeling of PPV, Beljonne *et al.*[25] included electron-electron interactions besides electron-phonon interactions. The inclusion of electron-electron interactions leads to splitting of singlet and triplet, both energetically and in terms of radius. Beljonne *et al.* have found the exchange energy, the energy difference between triplet and singlet, to be 0.6-0.7eV, and they also found the triplet to be more localized than the singlet. These estimates for PPV was done by extrapolating from phenylenevinylene oligomers, where oligomers are short chains of molecular subunits as opposed to the long chains, polymers. The extrapolation was done using oligomers with 2-5 subunits.

2.5 Transfer Mechanisms

Energy can be transferred from an excited polymer chain to other chains in the bulk around it. Three energy transfer mechanisms will be discussed, namely trivial, Förster, and Dexter.

2.5.1 Trivial

The energy transfer is named trivial or radiative if the transfer occurs through exciton decay in the donor molecule leading to emission of light which is absorbed by the acceptor molecule. That is, the two steps involved are as follows:

$$D^* \rightarrow D + h\nu,$$
$$h\nu + A \rightarrow A^*.$$

For this transfer mechanism to be effective, two requirements are particularly important. First, the acceptor has to have high extinction coefficient, leading to high absorption of light. Second, there has to be spectral overlap between the

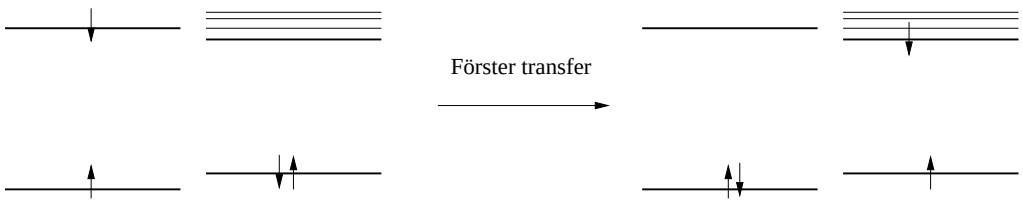

Fig. 2.13: Left: The initial state with the spin state of the electrons indicated by arrows. Right: The final state, after Förster energy transfer.

emission from the donor and absorption in the acceptor, that is the light emitted from the donor has to be absorbed by the acceptor.

2.5.2 Förster

The Förster transfer mechanism is a radiationless energy transfer. It does not involve any emission from donor or absorption in the acceptor, but transfer energy through Coulomb interaction between dipoles in donor and acceptors. It was first described by Förster in 1948[26] from whom it is named.

The excited donor molecule generates an oscillating dipole, which induces an alternating electric field. This alternating electric field induces a oscillating dipole in the acceptor and transfer energy from donor to acceptor, but only if the alternating electric field is in resonance with an electron in the acceptor, see Fig. 2.13. Due to the resonance requirement this transfer mechanism is occasionally named Förster Resonance Energy Transfer (FRET). Since the excited electron in the donor molecule decay to the ground state, Förster transfer is only possible for singlets. The efficiency of the Förster transfer process depends on a number of factors. First the relative orientation of the two dipoles in donor and acceptor. Second the spectral overlap between emission in the donor and absorption in the acceptor. Third the distance between the acceptor and the donor. The inducing dipole field in the donor molecule varies as R^{-3} of the distance R between donor and acceptor and so does the induced dipole field in the acceptor molecule. Therefore the transfer rate and the efficiency varies as R^{-6}. The relative orientation of the two dipoles has also impact on the transfer rate. According to Förster the transfer rate is

$$\kappa_F(R) \propto \frac{K^2}{R^{-6}},$$

where K is an orientation factor of the molecules. The transfer rate can also be related to the exciton lifetime if no energy transfer occurs τ and a characteristic radius or Förster radius R_0 by[27]

$$\kappa_F(R) = \frac{1}{\tau}\left(\frac{R_0}{R}\right)^6.$$

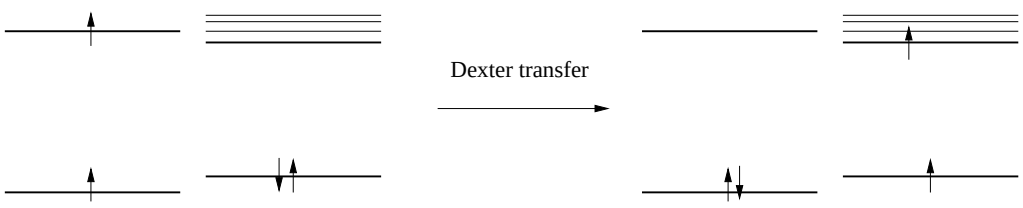

Fig. 2.14: Left: The initial state with the triplet state of the electrons in donor indicated by arrows. Right: The final state, after Dexter energy transfer, with triplet state in acceptor.

The Förster energy transfer has a long range of $\approx 10nm$. If the energy transfer is to an acceptor with no radiative decay, the process is termed quenching.

2.5.3 Dexter

The Dexter transfer mechanism is also a radiationless energy transfer. Dexter first described the process which involves tunnelling of electrons between acceptor and donor in 1952[28]. The energy transfer involves two tunnelling processes between the donor and accepter molecules, both of the excited electron from the donor molecule to the acceptor molecule and of a non-excited electron from the acceptor molecule to the donor molecule, see Fig. 2.14. The two tunnelling processes takes place simultaneously or as a two step process. Because the energy transfer involves tunnelling, the probability of the transfer and thus also the transfer rate depend exponentially on the distance between the to molecules. According to Dexter the transfer rate is

$$\kappa_D \propto \exp\left(-\frac{2R}{L}\right), \tag{2.11}$$

where R is the distance between donor and acceptor and L is the effective average Bohr radius of the excited state in the donor and the unexcited state in the acceptor. Another consequence of the tunnelling involved is the short range ($\approx 4nm$) of Dexter transfer, that is shorter than Förster transfer.

Another consequence of the energy transfer being a tunnelling process, is that triplets can also transfer energy from donor to molecule, because the transfer exchange the actual electrons, rather than transfer the energy through a decay process. The ability to transfer triplets has lead several groups to suggest using Dexter energy transfer to harvest the nonradiative triplets[29, 30]. The polymer is doped with a phosphorescent complex which act as acceptor in the transfer process. The complexes used are based on heavy metal atoms like iridium and platinum. These heavy metals mix the singlets and triplets through spin-orbit coupling, and hereby making light emission possible through a spin flip. Although the Dexter transfer mechanism is capable of transferring singlets, the transfer of singlets are dominated by Förster transfer due to the longer range of the latter.

2.6 Luminescence

In the process of photoluminescence (PL) excitons are generated through absorption of light. Hence, the excitons generated through PL will be able to decay through the same transition as it was excited and therefore all excitons generated through PL will be singlets. However, not all singlets decay radiatively and thus the PL efficiency is not 100%. It has been found that impurities in PPV reduces the PL efficiency[31]. The impurities enhances the non-radiative decay and hereby leads to the reduction in PL efficiency or quenching. These non-radiative decay can be caused by breaking of the charge-conjugation symmetry.

Electroluminescent devices with CP are fabricated as devices with organic molecules, with the light emitting polymer sandwiched between a hole-injecting anode with a high workfunction and a electron-injecting cathode with a low workfunction. In the present work the anode is at all times ITO or a hole injecting polymer (See Chap. 3) whereas the cathode is metals like aluminum and calcium.

Metal atoms evaporated onto the polymer generally lead to a formation of covalent bonds. However, it does not form a sharp metal polymer interface. In the interface between metal and polymer metal atoms diffuse into the polymer layer approximately $2-3nm$[32]. In the case of Ca cathode an interfacial oxide layer, which is insulating, is formed upon reaction with oxygen from either the polymer or the surrounding environment. The thickness of this oxide layer was also found to be in the $2-3nm$ range[32].

Electroluminescence involves exciton formation in the light emitting polymer layer and the subsequent exciton decay. The excitons are formed in the polymer through charge injection of holes and electrons, transport of these charges and the capture of electrons and holes by one another to form the excitons. In light generation through exciton decay the singlet to triplet ratio is of great importance, because only singlet decay radiatively.

It is important to have injection and transport of electrons and holes well balanced or the majority charge carrier (electron or hole) will result in a current of charges which cannot capture a charge of the opposite type to form an exciton. That is, unbalanced injection and transport will lead to low exciton formation efficiency η_{ce} defined as the number of excitons formed per injected electron-hole pair. The upper limit of the efficiency of the device is given by the balancing factor b

$$\begin{aligned} b &= B_C - B_A \\ &= C_A - C_C \end{aligned}$$

with B_C and B_A being the electron current fraction of the total current at cathode and anode, respectively, and C_A and C_C are the hole current fraction at anode and cathode, respectively. By balancing the injection and transport it is also possible to control position of the recombination zone which is of great importance to

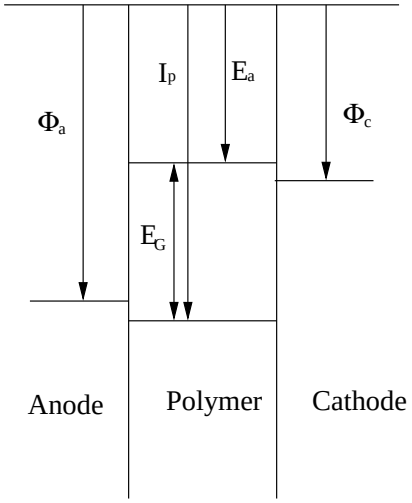

Fig. 2.15: Energy level diagram of a single layer device. Ionization potential and electron affinity of the polymer and workfunctions of the cathode and anode determine the injection barriers.

the efficiency of the radiative decay of excitons. The efficiency of the charge injection is highly dependent on the interfaces between contacts and polymer, see Fig. 2.15. There is a barrier toward hole injection which originates from a mismatch between the workfunction of the anode and the ionization potential of the polymer. Electron injection is suppressed by a similar barrier due to mismatch between the workfunction of the cathode and the electron affinity of the polymer. The height of these barriers are given by:

$$\begin{aligned} \Delta_h &= I_p - \Phi_a, \\ \Delta_e &= \Phi_c - E_a, \end{aligned}$$

where Δ_h and Δ_e are the hole and electron barriers, respectively, I_p and E_a are the ionization potential and electron affinity of the polymer and Φ_a and Φ_c are the workfunctions of the anode and cathode, respectively. In case of positive values of Δ, the contact is termed a blocking contact and if Δ is negative, that is the charges are free to flow into the polymer, the contact is termed ohmic. The anode (ITO) used in present work result in a relatively small barrier and consequently efficient hole injection. However, the choice of cathode between Al and Ca has great effect on electron injection, because the workfunctions of the two metals are $\Phi_{Al} = 4.3eV$ and $\Phi_{Ca} = 2.9eV$, respectively, resulting in a much higher barrier between Al and polymer. If the contact is a blocking contact charge injection occurs by overcoming the barrier through either thermionic emission or Fowler-Nordheim tunneling. The current density of holes and electrons in case

of thermionic emission $J^T_{e/h}$ is given by[33]:

$$J^T_{e/h} = A^* T^2 \exp\left(-\frac{\Delta_{e/h}}{k_B T}\right), \tag{2.12}$$

where A^* is the Richardson constant, T is the temperature and k_B is the Boltzmann constant. If the charges (holes or electrons) are injected through field emission or Fowler-Nordheim tunneling, the current density $J^{FN}_{e/h}$ is given by[34]:

$$J^{FN}_{e/h} = AE^2 \exp\left(-\frac{-4\sqrt{2m}\Delta^{2/3}_{e/h}}{3\hbar eE}\right), \tag{2.13}$$

with A being the tunneling coefficient, E the electric field, m the electron mass, and $\hbar$ Planck's constant. The electric field lowers the barrier by the Schottky effect by a factor of $\exp(\sqrt{E})$. For both electrons and holes the injection current density is at low electric fields ($< 5 \times 10^5 \frac{V}{m}$) controlled by thermionic emission(2.12), whereas at high electric fields ($> 5 \times 10^5 \frac{V}{m}$) it is controlled by Fowler-Nordheim tunneling(2.13).

Charges are transported in polymers through intrachain transport along the chain and interchain hopping, with the interchain hopping being the limiting factor. The current density of this transport of electrons and holes is given by the following expression:

$$J^{\mu}_{e/h} = \rho_{e/h} e \mu_{e/h} E, \tag{2.14}$$

where $\rho_{e/h}$ is the density of electrons or holes, e is the elementary charge, and $\mu_{e/h}$ is the mobility of electrons or holes due the the electric field E. The assumption that interchain hopping is the limiting factor for charge transport has been confirmed by Chen *et al.*[35] who found large mobilities along the polymer chain even across conjugation breaking defects. It was found that these defects do not seem to confine the charge carriers. Therefore the mobility can be greatly increased by aligning the chains along the direction of carrier transport. The overall current can thus be limited by either charge injection at either contact or by inefficient transport through the polymer. This has been investigated by Blom *et al.*[34] using a series of single carrier and two carrier devices. Single carrier devices are devices with either two high workfunction electrodes or two low workfunction electrodes, resulting in an inefficient electron or hole injection. Two carrier devices are devices with efficient injection of both carriers making exciton formation decay possible. Through analysis of hole-only devices with ITO and Au electrodes it was found that the hole current is space-charge limited without any indications of traps. The charge density J^{SC}_h is given by:

$$J^{SC}_h = \frac{9}{8}\epsilon \mu_h \frac{V^2}{L^3},$$

with ϵ being the permittivity of the polymer, V the applied voltage, and L the thickness of the polymer film. A similar analysis of electron-only devices with Ca electrodes on either side was performed showing that electrons are trapped in PPV resulting in a linear relationship between current density and applied voltage. However, above a critical voltage the traps become filled and the electron current density becomes space-charge limited. Using ITO as hole injecting electrode and Ca as electron injecting electrode in a PPV device results in small barriers towards charge injecting making the contacts practically ohmic. Generally it has been shown that contacts with small barriers $\Delta_{e/h} \leq 0.3eV$ are practically ohmic[36]. The hole mobility as defined in (2.14) is generally dependent on both electric field and temperature. The electric field dependence is found to be:

$$\mu_h(E) = \mu_h(0) \exp\left(\frac{E}{E_0}\right),$$

where $\mu_h(0)$ is the zero field mobility and E_0 is a characteristic electric field. The electric field dependence is related to the transport in disordered materials such as CPs. In the work by Blom *et al.*[37] it was found that there is also a temperature dependence of the mobility. The zero field mobility was found to be:

$$\mu_h(0) = \mu_h^0 \exp\left(-\frac{\Delta}{k_B T}\right),$$

with Δ being the activation energy.

Transport in polymers are often unbalanced due to difference in hole and electron mobilities, with the hole mobility being the higher. The recombination profile, that is, where in the device electrons and holes capture one another and subsequently recombine, is largely determined by the ratio of the charge mobilities and not the injection rates[33]. If there is unequal electron and hole mobility, the highest recombination occurs at the electrode which injects the charges with the lowest mobility. In this case it is preferred to have lowest barrier towards injection of the slowest charge to achieve the most efficient device. All these considerations are complicated by the electric field dependence of both mobility and barrier height making the balancing factor electric field dependent. However, it was found by Malliaras *et al.*[33] that as the voltage is increased the injection and transport tends to become better balanced and the balancing factor b approaches unity.

Once light is generated in the polymer through singlet exciton decay the efficiency of the out-coupling becomes a concern. The out-coupling efficiency ξ, that is how large a fraction of the generated light escapes the device, is defined as:

$$\eta^{ext} = \xi \eta^{int},$$

where η^{ext} is the external efficiency and η^{int} is the internal efficiency. This holds for both PL where the efficiencies are defined as the number of photons generated

per absorbed excitation photon and EL where the efficiencies are the number of photons per injected electron-hole pair. In the simplest case where emission intensity is constant in all directions the out-coupling efficiency can be calculated as[38]:

$$\xi = 1 - \sqrt{1 - \frac{1}{n^2}} \approx \frac{1}{2n^2},$$

where n is the refractive index of the polymer. However, Kim *et al.*[38] and Cao *et al.*[39] have both found this efficiency to be too low. Both found efficiencies up to:

$$\xi = \frac{1.2}{n^2}.$$

In the work by Kim *et al.* this was investigated further, and it was concluded that in-plane dipoles increased the efficiency as does the metal electrode in the device which acts as a reflector due to optical interference.

Like impurities in PPV, metal-polymer interfaces in EL devices lead to enhancement of the non-radiative decay of singlet excitons[40]. Due to this it is important to move the recombination zone away from the metal contacts used in EL devices. The energy from the non-radiative decay is transferred to the metal and scattered into the bulk to phonons and impurities. The lifetime of the excited state was also reduced in close proximity to the metal. The energy is transferred through Förster energy transfer[41]. Excitons are mainly formed near the metal cathode, due to low electron mobility which enhances the non-radiative decay. However, as voltages are increased the electron and hole mobilities are balanced, resulting in the recombination zone to move away from the metal cathode. This behavior has been demonstrated experimentially in different PPV derivatives[42, 43]. The range of the quenching behavior by the metal cathode has been estimated to be up to $60nm$[44].

The metal mirror also leads to a oscillatory dependence of the efficiency and lifetime of the radiative decay on the thickness of the emitting layer. This oscillatory dependence is due to interference between light emitted directly out of the polymer and light reflected by the metal mirror. This interference also changes the emission spectrum because the interference is obviously wavelength dependent. This effect has been explored with a thin (3nm) Al film and a thicker (35nm) Al film[44]. The thin Al film still quench the luminescence, but does reflect enough to give different emission spectrums for different polymer thickness which the thicker Al film does.

2.7 Spin Statistics

As mentioned earlier simple spin statistics predict the radiative singlet formation to occur in only 25% of all excitons. However, the assumption that simple spin

statistics are enough to estimate the triplet to singlet formation ratio has been challenged both theoretically and experimentally[39, 45, 46, 47].

Experimentally this has been challenged by comparing the efficiencies of photoluminescence η_{PL} and electroluminescence η_{EL}. The PL efficiency can be described by the following product:

$$\eta_{PL} = \eta_{sr}\eta_{ps}, \tag{2.15}$$

where η_{sr} is the number of radiative singlets per total singlets, and η_{ps} is the number of singlets formed per exciton in PL. Similarly the EL efficiency can be described as a product:

$$\eta_{EL} = \eta_{sr}\eta_{es}\eta_{ce}, \tag{2.16}$$

with η_{es} being the ratio between singlets and excitons in EL and η_{ce} is the number of excitons formed per injected charge carriers. Not all singlets decay radiatively, therefore $\eta_{sr} < 1$. It is η_{es} which simple spin statistics predicts to be 0.25. According to Greenham *et al.*[48] the efficiency of the radiative singlet decay used in both (2.15) and (2.16) is:

$$\eta_{sr} = \frac{\tau}{\tau_r}, \tag{2.17}$$

where the lifetime of the singlet is defined by $\tau^{-1} = \tau_r^{-1} + \tau_{nr}^{-1}$ and τ_r and τ_{nr} is the radiative and non-radiative lifetimes respectively. For (2.17) to hold Greenham *et al.* assumed both radiative and non-radiative decays are monomolecular processes with decay rates of $\kappa_r = \tau_r^{-1}$ and $\kappa_{nr} = \tau_{nr}^{-1}$ respectively. Greenham *et al.* measured a PL efficiency of $\eta_{PL} = 0.27$ and a PL lifetime of $\tau = 320ps$. With the lifetime of radiative singlets of $\tau_r = 1.2ns$ measured by Yan *et al.*[31], this gives $\eta_{sr} = 0.27$ and therefore η_{ps} has to be close to unity. These findings have been confirmed by Harrison *et al.*[49], however, they also found this was only the case for a pristine conjugated polymer. In oxidized PPV defects introduces non-radiative decay channels reducing the PL efficiency , particularly at high excitation energies.

The assumption that all excitons formed by PL are singlets has also been confirmed in photovoltaic measurements[50]. In this work Halls *et al.* estimated the exciton diffusion range, that is the range an exciton may move before decaying, was estimated to 6-8nm from a photocurrent measurement. Assuming that all excitons created by photon absorption are singlets they presented an exciton diffusion model predicting a similar exciton diffusion range. This leads to the conclusion that all excitons created by photon absorption indeed are singlets.

Because all excitons formed in PL are singlets, the ratio:

$$\frac{\eta_{EL}}{\eta_{PL}} = \frac{\eta_{es}\eta_{ce}}{\eta_{ps}} \simeq \eta_{es}\eta_{ce}$$

should have a upper limit of 0.25 if $\eta_{es} = 0.25$. This is, however not the case as demonstrated by Cau *et al.*[39]. They demonstrated a ratio as high as 0.50,

indicating either a low exciton binding energy or a higher probability of forming singlets than triplets, because triplet to singlet conversion is unlikely in these polymers. Both efficiencies were measured on the same device with a PPV derivative blend with an electron transport material (2-(4-biphenyl)-5-(4-tert-butylphenyl)1,3,4-oxidiazole), Bu-PDB. The electron transport material increases the efficiency of EL, but has no effect on PL efficiency. The increase in EL efficiency is due to better balance of electron and hole injection. In the works by Kim *et al.*[38] it was found that the singlet formation ratio η_{es} was in the range $0.35 - 0.45$.

As mentioned in Sec. 2.4 the exciton binding energy of PPV is $0.6 - 0.7eV$ ruling out the possibility of thermalized triplet excitons to luminescence. The other possibility, that the singlet is formed with a higher probability can be attributed to a difference in formation cross-section. The efficiency of singlet formation in EL η_{es} can be related to the cross-sections by:

$$\eta_{es} = \frac{\sigma_s}{\sigma_s + 3\sigma_t}, \tag{2.18}$$

where σ_s and σ_t are the formation cross-sections of the singlet and the triplet respectively. If the cross-sections of singlets and triplets are equal, the efficiency would be 0.25 as predicted by simple spin statistics. To achieve the efficiency of 0.50, which is the lower limit in the measurements by Cau *et al.* the singlet cross-section would have to be $\sigma_s = 3\sigma_t$. In the theoretical work by Shuai *et al.*[45] it was found that the cross-section indeed is greater for singlets than triplets. Wohlgenannt *et al.* investigated a variety of conjugated polymers with photoinduced absorption and found the singlet-triplet cross-section ratio $\frac{\sigma_s}{\sigma_t}$ to range from 1.8 to 5.0, that is in all cases the singlet formation probability in all cases exceeded 0.25. In the case of PPV the ratio was found to be 2.2 giving $\eta_{es} = 0.42$, which is in reasonable agreement with the findings by Cau *et al.* and Kim *et al.*

The mentioned experimental methods investigated the lower limit of the singlet formation probability η_{es}. Wilson *et al.*[47] have demonstrated a method to determine the absolute probability, rather than the lower limit. They used a polymer containing platinum (Pt), and because of the heavy Pt-atom, radiative emission from triplet exciton decay is possible. In this case the singlet formation probability can be measured as

$$\eta_{es} = \frac{c_{PL}}{c_{EL}}, \tag{2.19}$$

where c_{PL} and c_{EL} are the fractions of photons emitted from triplet exciton decay to photons emitted from singlet exciton decay in PL and EL respectively. For this to hold, the quantum yield of the intersystem crossing has to be close to unity, which indeed is the case for the polymer in question[51]. It is possible to distinguish triplets and singlets from one another because emission occurs at

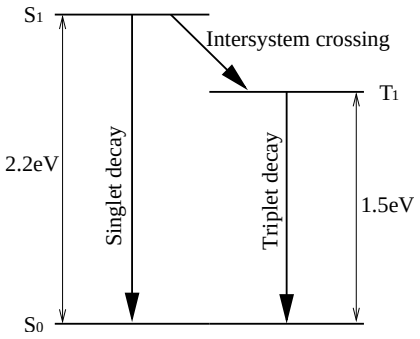

Fig. 2.16: Energy levels in the polymer used in ref. [47].

different energies, triplets at $\approx 1.5eV$ and singlets at $\approx 2.2eV$ as illustrated in Fig. 2.16. In the work by Wilson *et al.* a number of samples was tested both with monomers and polymers with varying film thickness, applied electric fields, and at different temperatures. The overall trend was that thickness, applied electric fields and temperatures had no effect on the singlet formation probability, whereas monomers followed simple spin statistics and polymers did not. The importance of the size of the molecules is confirmed by measurements of the singlet to triplet formation ratio of 1 to 3 in Alq_3[52]. The differences in efficiency between small molecules (monomer and Alq_3) and large molecules (polymer) are due to sizes of the compounds. In small molecules electron hole capture occurs solely through the spin-independent Coulomb interaction between holes on one molecule and electrons on another. It is a purely intermolecular process and it is spin-independent. In large molecules on the other hand, the electron hole capture also occurs on a single molecule. This leads to overlap between electron and hole because of the delocalized nature of the electron and hole orbital and the interaction is no longer spin-independent. Because the interaction is spin-dependent the electron hole capture is as well. As mentioned in Sec. 2.4 the singlet has longer extension than the triplet. The electrons and holes injected into the polymer are transported through the polymer through hopping from molecule to molecule. Because of the shorter extension of the triplets they are more likely to hop to other molecules before the electron and the hole capture one another to form an exciton.

Another approach to measure the singlet to triplet ratio was developed by Lin *et al.*[43]. This method does not require a heavy atom in the backbone of the polymer, because it does not rely on radiative decay of triplets, and can therefor be used on all CPs and not only those with heavy atoms. If γ is the triplet to

singlet ratio, (2.18) can be written as:

$$\eta_{es} = \frac{1}{1+\gamma}. \tag{2.20}$$

If the cross-sections are equal for singlets and triplets the triplet to singlet ratio is $\gamma = 3$. By measuring the triplet-induced absorption in electric- and photoexcited polymers, Lin *et al.* determined the triplet to singlet ratio, using:

$$\gamma = \frac{\rho_T^{EL}\tau_S}{\rho_T^{PL}\tau_{ISC}}, \tag{2.21}$$

where ρ_T^{EL} and ρ_T^{PL} are the density of electric- and photoinduced triplets, respectively, τ_S and τ_{ISC} are the lifetime of the singlet and intersystem crossing, respectively. It was found that the ratio is not constant, but highly electric field dependent. The ratio was decreasing and singlet formation probability was increasing with increasing electric field.

Part II

Materials

Chapter 3

Charge Injecting Materials

Organic charge injecting materials are used to improve the efficiency and lifetime of devices. These materials also open up for the possibility of make flexible displays with a organic anode. It was first introduced by Gustafsson *et al.* who used polyaniline (PANI) coated on glas or plastic (poly(ethylene terephthalate)) substrates as hole injecting contact[53], the chemical structure is illustrated in Fig. 3.1. PANI has also been used as an overlayer on top of ITO resulting in a decrease in operating voltage of $\sim 30 - 50\%$ and increase in device efficiency of $\sim 30 - 40\%$ compared to device with ITO alone[54]. These device improvements are due to a lower hole injection barrier because PANI has a slightly higher workfunction. The lowering of the hole barrier is determined by a Fowler-Nordheim analysis of a hole-only device. One disadvantage of PANI as hole injecting electrode is that the thickness has to low to keep the PANI transparent, however, the low thickness results in a high resistance. Combining the advantages of both materials, PANI and ITO, it is possible to get a contact with high workfunction and low resistivity. Doping the PANI with sulfonic acids such as camphor sulphonic acid (CSA) or polystyrenesulfonic acid (PSS), see Fig 3.2 for chemical structure, makes PANI soluble in common organic solvents as well as water[55]. The PSS is a polymer whereas CSA is a monomer, that is the dopants can be either polymer or monomer. The use of a soluble polymer compared to an insoluble polymer has two advantages. First, the ease of processing and second the

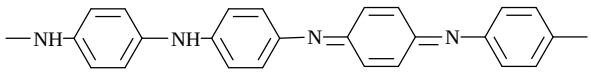

Fig. 3.1: The emeraldine state of polyaniline or PANI.

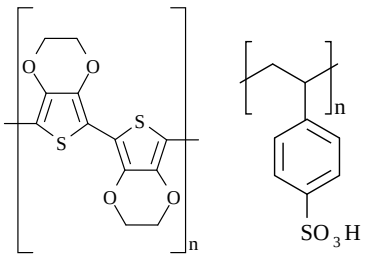

Fig. 3.2: Left: Poly(dioxyethylene thienylene) or PEDOT. Right: Polystyrenesulphonic acid or PSS.

precursor polymerization often involves an oxidizing agent which is undesirable on the device.

A different type of charge injecting polymer are the polythiophenes such as poly(dioxyethylene thienylene) (PEDOT), see Fig. 3.2. It is PEDOT doped with PSS, termed PEDOT:PSS, desolved in water which are used in the present work. A study of the two polymers (PANI and PEDOT) has revealed that both materials have improved performances compared to ITO, independent of dopant and solvent[56]. This study also showed that the physical contact between polymer and electrode was improved by PEDOS:PSS resulting in enhanced adhesion of the polymer to the electrode. As it is the case for PANI, PEDOT also has a slightly higher workfunction than ITO making the hole injection barrier smaller and the device more efficient. Furthermore the devices with a polymeric dopant in the hole injection polymer have higher efficiency than devices with a monomer dopant. It is believed that this is because the free monomer dopants diffuse into the light emitting polymer and act as quenchers whereas the polymer dopants are bound to the hole injecting polymer.

As mentioned there is also an increase in lifetime when using a polymer hole injecting polymer compared to ITO. This is because the oxygen from ITO tends to oxidize the polymer which introduces defects in the polymer breaking the conjugation[57, 58]. The oxidation is accelerated during device operation due to photo-oxidation. The ITO was identified as the oxygen source, by examining IR absorption spectrum of a ITO/polymer interface before and after UV exposure. This revealed a large change in absorption which could be attributed to a change in oxidation states in the ITO making ITO a likely source for oxidation of the polymer. The increase in lifetime is also seen in bilayer hole injecting devices, such as PEDOT:PSS on ITO because the polymer act as a barrier towards the oxidation from ITO. The lifetime of the polymer anode devices are also increased compared to ITO based devices because the tend to be more planar. Nonplanar anodes leads to an uneven charge injection with high injection currents at spots. These spots with high injection currents are more likely to break down and give

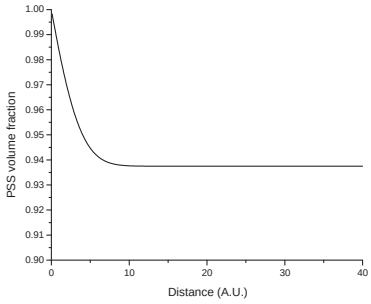

Fig. 3.3: The volume fraction of PSS in PEDOT as a function of distance from the surface.

shorts, eventually responsible for the break down of the device.

Finally using hole injecting polymers gives more reproducible devices than devices with ITO, because the workfunction of ITO can vary $\pm 0.5eV$ depending on how it is prepared[56]. It is also susceptible to water absorption and oxidation, which also can affect the performance of the device. After spincoating of the polymer based hole injecting electrode the samples are heated to at least 100^oC for $30min$ or more to remove the solvent. Any remaining solvent will have a negative influence on the device, especially in the case of water. The importance of heat treatment of the anode prior to applying the light emitting polymer is strengthen by the polymer anodes sensitivity to excess water[59].

The blends of polyanilines or polythiophenes and sulfonic acids give complex materials with an nonuniform distribution of hole injecting polymer and acid, with one of the two dominating the surface and a uniform distribution in the bulk. According to Jukes *et al.*[60] this is due to the difference in surface energy of the two compounds in the blend where the compound with the lower surface energy will diffuse to the surface. In the case of PEDOT:PSS it is PSS which has the lowest surface energy resulting in an interface with only PSS. The volume fraction of PSS $\delta(z)$ can be described as:

$$\delta(z) = \delta_0 + (\delta_1 - \delta_0)\frac{\text{erfc}\left(\frac{z+\Delta}{\sigma}\right)}{\text{erfc}\left(\frac{\Delta}{\sigma}\right)}, \tag{3.1}$$

where δ_0 is the bulk volume fraction, δ_1 is the surface volume fraction which in this case is unity, Δ is an offset and σ describes the width of the interface. The volume fraction of PSS as a function of distance from the surface with a pure PSS surface ($\delta_1 = 1$) and a bulk fraction $\delta_0 = 15/16$ is seen in Fig. 3.3. The pure PSS interface has been confirmed experimentally by Greczynski *et al.*[61]. It was found by Jukes *et al.* that the thickness of this pure PSS interface layer can be controlled by subsequent heat treatment of the hole injecting polymer. Time and temperature of the heat treatment and the PEDOT to PSS ratio in the

bulk determined the thickness. This can be used to make more efficient devices because the PSS acts as an efficient hole barrier controlling the hole injection. This way the hole injection can be chosen to match the electron injection making the charge injection balanced resulting in an more efficient device. This was demonstrated experimentally by Jukes *et al.* by investigating the influence of the PEDOT to PSS ratio on device efficiency. It was found to peak at a PEDOT to PSS ratio of $1 : 15$ confirming formation of an interface layer because this peak cannot be explained by bulk effects.

Chapter 4

Light Emitting Polymers

4.1 Poly(p-phenylene vinylene)

As mentioned in Sec 2.3 PPV was the first CP to show EL, first in the unmodified, insoluble PPV and second in the modified, soluble MEH-PPV. The side groups attached to the backbone in MEH-PPV to make it soluble also affected the luminescent properties of the polymer. The EL spectrum from a MEH-PPV device, where the polymer was spun from a $3\frac{mg}{ml}$ solution at $700RPM$, and with Ca/Al as electron injector and ITO/PEDOT:PSS as hole injector is depicted in Fig. 4.1. The positions of the peaks has been determined by examining the negative second derivative of the EL spectrum. The peak at $587nm(2.11eV)$ is due to a purely electronic transition, termed the 0-0 transition, whereas the peak at $640nm(1.94eV)$ involves coupling of the electronic transition to molecular vibrations or phonons, termed the 0-1 transition, in the polymer chain. The energy of the phonon is

$$E_{ph}^{MEH-PPV} = 2.11eV - 1.94eV = 0.17eV = 1410cm^{-1},$$

which is in agreement with photoluminescence measurements [62] and electroabsorption measurements[63]. The phonon is a double bond (C=C) stretching phonon, but low frequency phonons ($< 100cm^{-1}$) due to torsion of the phenylene ring are also involved in the luminescence process[64]. These low frequency phonons, however, cannot be resolved in the luminescence spectrum, but result in broadening of the peaks, both zero-phonon (0-0) and phonon coupled (0-1) transitions. The absorption spectrum of MEH-PPV has also been measured and the result is seen in Fig. 4.2. The second derivative of the absorption spectrum is included in Fig. 4.2 in order to determine the positions of the absorption peaks $525nm$ $(2.36eV)$ and $490nm$ (2.53eV). This confirms the emission measurements of the phonon energy and enables one to determine the Stokes shift $E_{Stokes}^{MEH-PPV} = 2.36eV - 2.11eV = 0.25eV$, i.e. the energy difference between

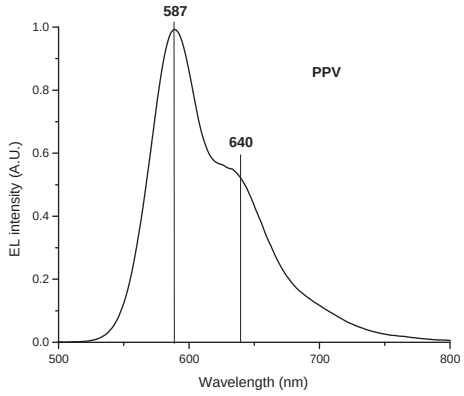

Fig. 4.1: The EL spectrum of a MEH-PPV device.

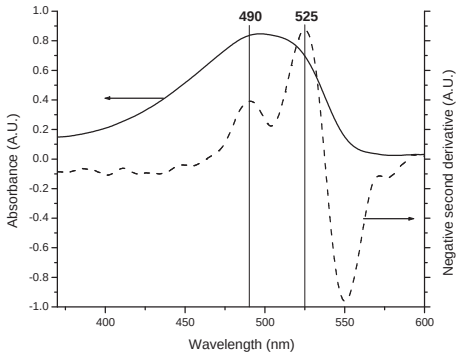

Fig. 4.2: The absorption spectrum and the negative second derivative of the absorption spectrum of MEH-PPV.

the zero-phonon absorption peak and the zero-phonon emission peak. The shift is due to relaxation of the excited state, lowering the energy of the excited state and thus also the energy gap involved in emission.

The IV characteristics of a $100nm$ thick MEH-PPV device with Ca and ITO electrodes is depicted in Fig. 4.3 with both linear and logarithmic scale. The graph on the left in Fig. 4.3 with linear scale demonstrates the diode behavior of the device with a turn-on voltage of $3.5V$. The graph on the right with logarithmic scale illustrates the presence of traps and a critical voltage of $3V$. Above the critical voltage the traps are filled and the current becomes trapfree. Increasing

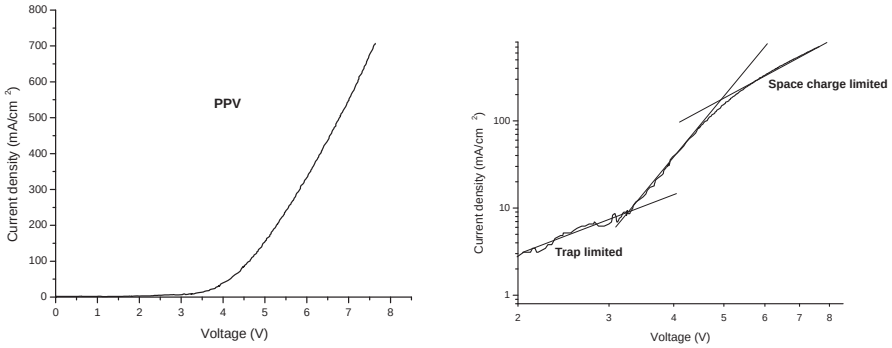

Fig. 4.3: The IV characteristics of a MEH-PPV device with linear scale (left) and logarithmic scale (right).

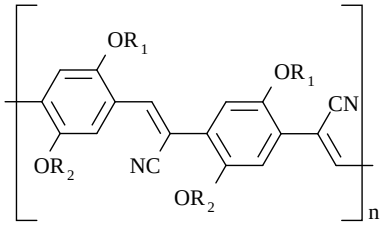

Fig. 4.4: The chemical structure of dialkoxy-substituted PPV with cyano-groups on the vinylene part of PPV (CN-PPV).

the voltage further, the current becomes space charge limited.

Since the first report of EL from PPV a number of PPV derivatives have been investigated to achieve luminescence at different wavelengths. One example of such PPV derivatives is dialkoxy-substituted PPVs with cyano-groups attached to the vinylene part of the polymer (CN-PPV), see Fig. 4.4. The addition of cyano-groups has no severe effect on the bandgap, which is mainly determined by the PPV backbone and the dialkoxy-substitutions. As it is the case for PPV without cyano-groups the dialkoxy-substitutions are also necessary to make the CN-PPV soluble. The effect of the cyano-groups is a lowering of the electron affinity of approximately $0.5eV$[65]. Because the bandgap is unchanged the ionization potential is also lowered. The lowering of the electron affinity and ionization potential is due to the electron withdrawing effect of the added cyano group. The same effect as was described in organic molecules in Chap. 1. Because of the lowering of the ionization potential devices with CN-PPV as light emitter and ITO as hole injector have a high barrier towards holes. On the other hand, the lower

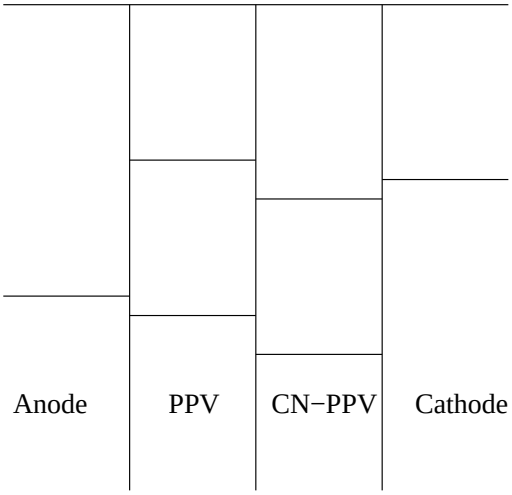

Fig. 4.5: A dual layer device with CN-PPV and PPV sandwiched between anode and cathode.

electron affinity lowers the electron injection barrier. Therefore devices made with CN-PPV are hole injection limited, which was confirmed by investigations showing the efficiency of devices based on CN-PPV can reach 0.2% independent of the choice of electron injecting electrode between Ca and Al[66]. These properties has been exploited in a dual layer device with CN-PPV and PPV as illustrated in Fig. 4.5. The device utilizes the low barriers towards hole and electron injection between the electrodes and PPV and CN-PPV, respectively, to achieve efficient charge injection. The difference in ionization potentials and electron affinity between PPV and CN-PPV results in barriers towards hole transport from PPV to CN-PPV and towards electron transport from CN-PPV to PPV. As a result the recombination is confined to the interface between the polymers increasing the device efficiency because quenching due to the metal electrodes is reduced. The confinement of the recombination zone is important in PPV because PPV has low electron mobility resulting in increased recombination near the metal electrode in single layer devices and thus quenching. This was investigated by Becker *et al.*[44] who indeed found an increase in device efficiency with increasing thickness of CN-PPV, that is the device efficiency increased as the recombination zone was move away from the metal electrode. The recombination at the CN-PPV/PPV interface involves tunneling across the barriers between the two polymers, resulting in a recombination zone of$\sim 20nm$[44]. The barriers also lead to a build up of charges at the interface making exciton formation more likely. The use of CN-PPV/PPV dual layer also have another advantage since effective electron injection from Al into CN-PPV is possible. Al is environmentally stable and therefore further encapsulation of the cathode is not necessary as it is the case for low workfunction metals like Ca.

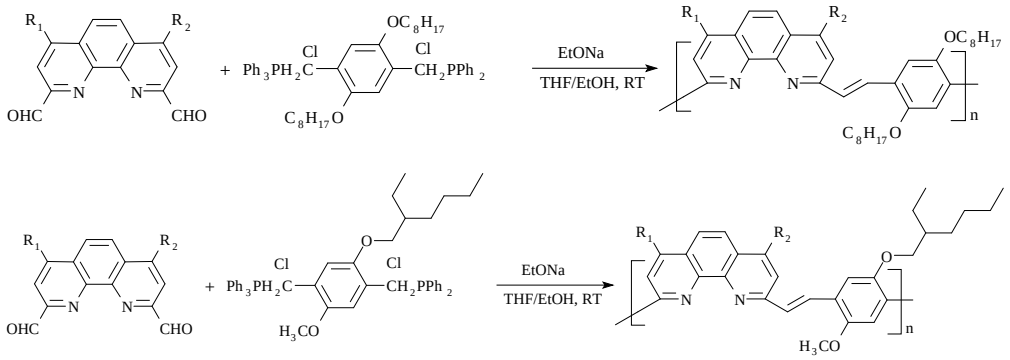

Fig. 4.6: The synthesis scheme and chemical structure of the four PPV copolymers.

Four other PPV derivatives have been synthesized and investigated with PL and EL measurements. The four derivatives are all copolymers, that is polymers with two or more monomers in the polymer backbone. The copolymers presented here all have phenanthroline as the second monomer besides phenylene vinylene, but with a variety of sidegroups to the phenanthroline and the phenylene. The synthesis schemes and the chemical structures of the final polymers are seen in Fig. 4.6. The upper part of Fig 4.6 illustrates the synthesis of Phen-DO-PPV and Bath-DO-PPV, where the difference between the two lies in the side groups of phenanthroline. The side groups R_1 and R_2 are H and phenylene in Phen-DO-PPV and Bath-DO-PPV, respectively. The lower part of Fig 4.6 illustrates the synthesis of Phen-MEH-PPV and Bath-MEH-PPV, where the side groups R_1 and R_2 are H and phenylene in Phen-MEH-PPV and Bath-MEH-PPV, respectively. The four copolymers were synthesized by incorporating the two different phenanthroline monomers and the two different phenylene vinylene monomers in the polymer chain via the Wittig condensation reaction and carefully purified.

PL measurements on the polymers in solutions are illustrated in Fig. 4.7. The PL measurements on the polymers were performed with an excitation wavelength of $390nm$ ($3.18eV$) using the frequency doubled output from a mode-locked Ti-Sapphire laser. The inclusion of phenanthroline in the polymer chain blue-shifts the emission significantly compared to MEH-PPV from $587nm$ to near $500nm$. The phenylene side groups on phenanthroline, however, seems to red-shift the emission slightly, since both Phen-DO-PPV and Phen-MEH-PPV have the first peak at shorter wavelengths than Bath-DO-PPV and Bath-MEH-PPV. The peak positions of the transitions without electron-phonon coupling (0-0) and the first transitions with electron-phonon coupling (0-1) are determined by examination of the negative second derivative of the emission spectrum and are listed in Table 4.1 along with the energy of the phonon in the 0-1 transition calculated as the

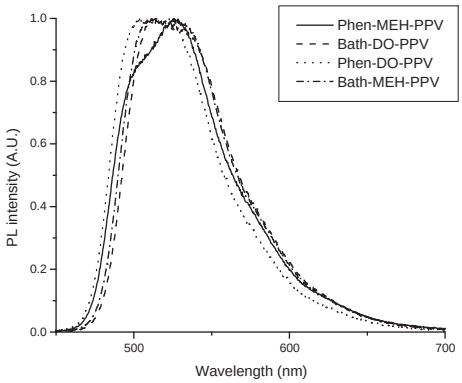

Fig. 4.7: PL measurements on the four PPV copolymers in THF solutions.

Polymer	0-0 transition	0-1 transition	E_{ph}
Phen-DO-PPV	$493nm$ $(2.52eV)$	$529nm$ $(2.34eV)$	$1422cm^{-1}$ $(0.18eV)$
Bath-DO-PPV	$502nm$ $(2.47eV)$	$539nm$ $(2.30eV)$	$1357cm^{-1}$ $(0.17eV)$
Phen-MEH-PPV	$493nm$ $(2.52eV)$	$531nm$ $(2.34eV)$	$1452cm^{-1}$ $(0.18eV)$
Bath-MEH-PPV	$500nm$ $(2.48eV)$	$539nm$ $(2.30eV)$	$1447cm^{-1}$ $(0.18eV)$

Table 4.1: The transitions involved in emission in a Eu-complex[67].

difference between the two transitions. The peak positions confirms the observation of a small blue-shift in Phen-DO-PPV and Phen-MEH-PPV compared to Bath-DO-PPV and Bath-MEH-PPV. The choice of side group to the phenylene vinylene does not affect the peak position significantly, however, there seems to be a stronger electron-phonon coupling in polymers with the MEH sidegroups, observed as a relatively higher intensity of the 0-1 transition peak in these polymers compared to the polymers with DO side groups. The phonon energies listed in Table 4.1 are all assign to double bond (C=C) stretching.

The EL spectrum from a device with Phen-DO-PPV sandwiched between a ITO/PEDOT:PSS anode and a Ca/Al cathode was recorded and illustratted in Fig. 4.8 along with the PL spectrum of Phen-DO-PPV. The device was manufactured with PEDOT:PSS spun from a 0.7% solution with $1000RPM$, heated to $130°C$ for 30 min, and the polymer spun at $700RPM$ from a $5\frac{mg}{ml}$ solution, and finally Ca and AL electrode was evaporated on top. It is observed that the

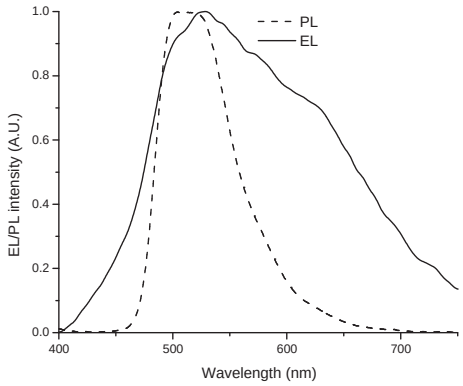

Fig. 4.8: EL measurements on a Phen-DO-PPV copolymer based device along with PL measurements on the same polymer in THF solutions.

first peak at $504nm$ $(2.46eV)$ seems to been the same in EL as in PL, however, additional peaks at longer wavelengths are introduced in the EL spectrum. These are assigned to excimer emission, that is emission due to interchain interaction between an excited polymer chain and a ground state polymer chain. A thorough description of the synthesis of these PPV based copolymers along with the results presented here have been published in Ref. [3].

Defects occur in polymers breaking the conjugation along the chain, see Fig. 4.9. These defects include cis-defects or twisting of the chain, saturation defects where the double bond in the vinylene part of PPV is turned into a single bonds by adding two extra hydrogen atoms, and oxidation or carbonyl defects where the double bond in the vinylene is turned into a single bond by replacing one of the hydrogen atoms with oxygen and adding one extra hydrogen atom to the other carbon atom. The extra hydrogen atoms in saturation and oxidation defects are out of plane. In saturation and oxidation defects the p_z conjugation is broken by saturation of the carbon atoms in the vinylene part of the molecule. In cis defects the p_z conjugation is broken because this defect involves a 144^o out of plane twist. These defects, however, do not lower the electron transport significantly as mentioned in Sec. 2.6. This is because the delocalized π-orbitals on either side of a defect are still connected.

4.2 Polyfluorenes

In the search for a blue emitting polymer the initial investigation was concentrated on poly(para-phenylenes), that is polymers where the backbone consisst of only phenylene rings. As it is the case for PPV, attaching side groups are

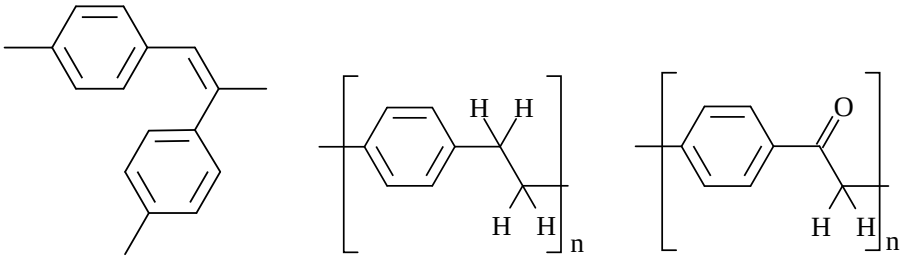

Fig. 4.9: Different types of defects, cis-defect (left), saturation defect (middle), and oxidation defect (right).

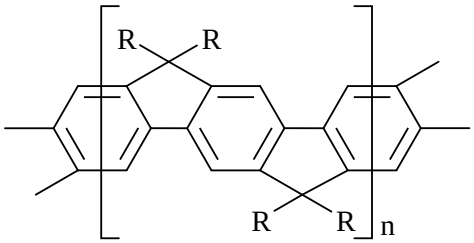

Fig. 4.10: The chemical structure of ladder-type poly(para-phenylenes) (LPPP).

necessary to make the polymer soluble. The drawback of this, however, is the torsion of the ring due to these side groups reducing the conjugation of the polymer and hereby the efficiency of the polymer. One solution to this is the use of ladder-type PPP (LPPP) with every phenyl ring bridged to the next making the polymer chain rigid and thus making torsion virtually impossible, see Fig. 4.10 for the chemical structure. A different type of rigid PPP based polymer are the polyfluorenes, which have phenyl rings bridged in pairs. EL from the polyfluorene, poly(9,9-bis(3,6-dioxaheptyl)-fluorene-2,7-diyl) (BDOH-PF), was reported by Pei and Yang[68] in 1996. Another example of a polyfluorene based polymer is poly(9,9-dioctylfluorenyl-2,7-diyl) (PF) which has a chemical structure as depicted in Fig. 4.11, and from which EL was first reported by Grice *et al.*[69] in 1998. The polyfluorene based polymers indeed have luminescence in the blue part of the spectrum as illustrated by the EL spectrum of a PF device in Fig. 4.12. In the device a $100nm$ thick layer of PF was spin coated from a $5\frac{mg}{ml}$ solution at $1500RPM$ on an ITO/PEDOT:PSS anode and a Al/Ca cathode was applied afterwards. The EL spectrum has three distinct peaks at $438nm$ ($2.83eV$), $465nm$ ($2.67eV$), and $495nm$ ($2.51eV$). The spacing is due to electron-phonon coupling

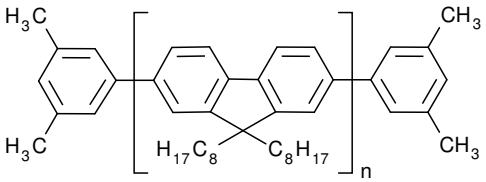

Fig. 4.11: The chemical structure of poly(9,9-dioctylfluorenyl-2,7-diyl) (PF).

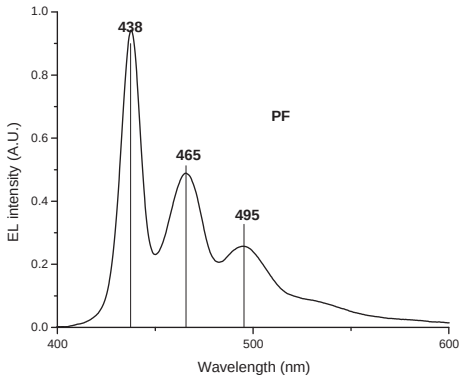

Fig. 4.12: The EL spectrum of a PF device.

with phonon energies of

$$E^{PF}_{ph,E,1} = 2.83eV - 2.67eV = 0,16eV = 1325cm^{-1},$$
$$E^{PF}_{ph,E,2} = 2.83eV - 2.51eV = 0,33eV = 2629cm^{-1}.$$

The second phonon energy $E^{PF}_{ph,E,2}$ is approximately the double of the first $E^{PF}_{ph,E,1}$ as expected. The $465nm$ peak is due to electron coupling to a double bond (C=C) streching phonon, whereas the $495nm$ peak is presumably due to coupling to two double bond (C=C) stretching phonons. It is notable how well resolved the individual peaks are compared to the peaks in PPV. This is due to the more rigid structure of PF reducing the vibrations due to torsion of the phenylene ring, which are responsible for the broadening of the peaks. The length and chemical composition of the side group do not control the luminescent properties of PF, but only serves as a means to render the polymer soluble. This is because

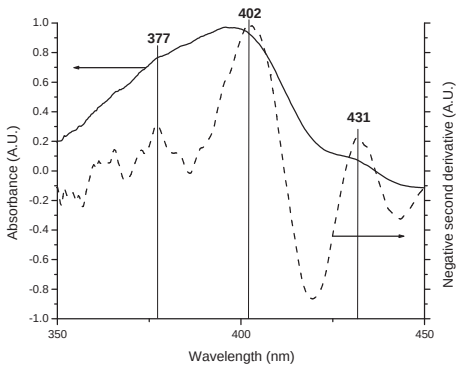

Fig. 4.13: The absorption spectrum and the negative second derivative of the absorption spectrum of a PF film on a glass substrate.

the side group is positioned away from the direct bond between the two phenyl rings, which are responsible for light emission.

The absorption spectrum of a PF film on a glass substrate has been measured as depicted in Fig. 4.13 along with the negative second derivative of the absorption in order to determine the peak positions in the absorption spectrum. With peaks at $431nm$ $(2.88eV)$, $402nm$ $(3.08eV)$, and $377nm$ $(3.29eV)$ it can be concluded that PF has a small Stokes shift of $E^{PF}_{Stokes} = 2.88eV - 2.83eV = 0.05eV$. From these peaks in the absorption spectrum the phonon energies in absorption can be determined as:

$$E^{PF}_{ph,A,1} = 3.08eV - 2.88eV = 0.20eV = 1674cm^{-1},$$
$$E^{PF}_{ph,A,2} = 3.29eV - 2.88eV = 0.41eV = 3323cm^{-1}.$$

Apparently it is different phonons which couple in absorption but the second phonon energy $E^{PF}_{ph,A,2}$ is still the double of the first $E^{PF}_{ph,A,1}$ and the $377nm$ peak is presumably due to coupling to two phonons. The low intensity of the peak without electron-phonon coupling at $431nm$ is due to strong electron-phonon coupling.

The ionization potential and electron affinity of PF have been determined by Campbell *et al.* to be $I_p = 5.8eV$ and $E_A = 2.6eV$, respectively[70]. The work function of calcium $W_{Ca} = 2.9eV$ matches the electron affinity quite well making electron injection efficient whereas hole injection is limited by a barrier. Because the hole injecting contact is the limiting factor, using ITO coated with PEDOT:PSS significantly improves the efficiency compared with ITO alone. Campbell *et al.* found an current increase of up to 4 orders of magnitude between pure ITO and PEDOT:PSS coated ITO, i.e. the electron injection becomes more efficient.

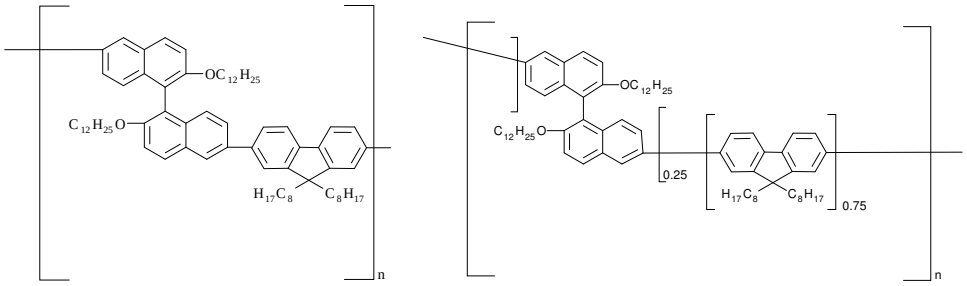

Fig. 4.14: Left: The chemical structure of P(BiNDO-FO). Right: The chemical structure of P(BiNDO-FO3).

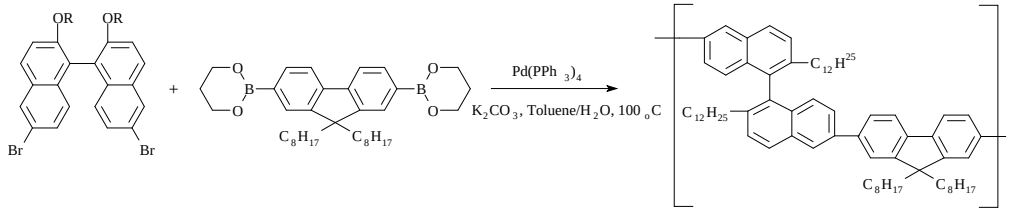

Fig. 4.15: The synthesis scheme of P(BiNDO-FO) and P(BiNDO-FO3).

Polyfluorenes have also been used in copolymers in order to tune the luminescent properties of the polymer. The two copolymer are Poly[(6,6'-(2,2'-didodecyloxyl)-1,1'-binaphtyl)-co-(9,9'-dioctylfluorene)], with P(BiNDO-FO) which has a equal ratio of fluorene monomer and binaphthyl monomer and P(BiNDO-FO3) which has three fluorene monomers for every binaphthyl monomer, see Fig. 4.14 for the chemical structures. EL from P(BiNDO-FO3) was first reported by Jiang *et al.* in 2000, where P(BiNDO-FO3) was demonstrated as an efficient blue emitter with a PL efficiency of 44% and with a double layer device an EL efficiency of 0.82% was achieved[71].

The two polymers were synthesized via a Suzuki coupling reaction of a binaphthyl dibromide and dioctylfluorene diboronic acid and carefully purified, the synthesis scheme is illustrated in Fig. 4.15. Devices with P(BiNDO-FO) and P(BiNDO-FO3) sandwiched between ITO and Ca/Al have been manufactured and EL spectra were recorded and are depicted in Fig. 4.16. The peaks are determined using the negative second derivative, which is particularly necessary in P(BiNDO-FO) where the peaks due to coupling to phonons are not as well resolved as in P(BiNDO-FO3) and PF. In the work by Jiang *et al.* a blue shift in the emission spectrum was found once introducing the binaphthyl monomer

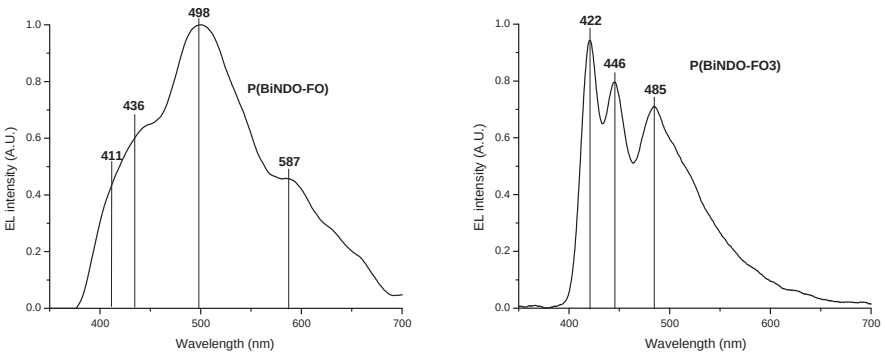

Fig. 4.16: Left: The EL spectrum of a P(BiNDO-FO) device. Right: The EL spectrum of a P(BiNDO-FO3) device.

in the polymer chain. It was believed that because of a large dihedral angle between the two naphthyl group in binaphthyl, the binaphthyl monomer breaks the conjugation, and shorter conjugation is known to blue shift the emission. The dihedral angle between the two naphthyl groups is between 60° and 120°, enough to break the conjugation. The phenomenon is confirmed by the EL spectrum of P(BiNDO-FO) which is blue shifted even further due to the presence of the conjugation breaking binaphthyl monomer between every fluorene monomer. The short conjugation length in P(BiNDO-FO), however, has the undesirable effect of making it a inefficient EL device. A similar blue shift in emission due to a conjugation breaking binaphthyl monomer has also been demonstrated in PPV[72].

With peaks at $411nm$ $(3.02eV)$ and $436nm$ $(2.84eV)$ in P(BiNDO-FO) and at $422nm$ $(2.94eV)$, $446nm$ $(2.78eV)$, and $485nm$ $(2.56eV)$ in P(BiNDO-FO3) the phonon energies are

$$\begin{aligned} E_{ph,E,1}^{P(BiNDO-FO)} &= 3.02eV - 2.84eV = 0.18eV = 1395cm^{-1}, \\ E_{ph,E,1}^{P(BiNDO-FO3)} &= 2.94eV - 2.78eV = 0.16eV = 1275cm^{-1}, \\ E_{ph,E,2}^{P(BiNDO-FO3)} &= 2.94eV - 2.56eV = 0.38eV = 3078cm^{-1}. \end{aligned}$$

The energies of the first phonon modes $E_{ph,E,1}^{P(BiNDO-FO)}$ and $E_{ph,E,1}^{P(BiNDO-FO3)}$ are both close to the phonon energy in PF indicating it is the same phonon mode which couple to the emission spectrum. The peak at $485nm$ in P(BiNDO-FO3), however, does not originate from coupling to two phonons as in PF but rather from coupling to a different phonon mode. The energy of the phonon matches the typical energy of a stretching C-H bond phonon[73].

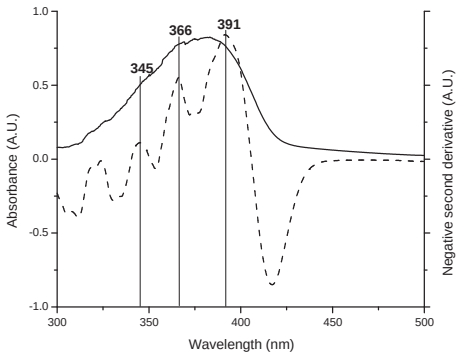

Fig. 4.17: The absorption spectrum and the negative second derivative of a P(BiNDO-FO3) film on a glass substrate.

The absorption spectrum of a P(BiNDO-FO3) film on a glass substrate has been measured and the spectrum is depicted in Fig. 4.17. From the positions of the peaks in the absorption spectrum of P(BiNDO-FO3) at $391nm$ $(3.17eV)$, $366nm$ $(3.39eV)$, and $345nm$ $(3.59eV)$ it can be concluded that the introduction of binaphthyl in the polymer chain result in an increase in Stokes shift to $E_{Stokes}^{P(BiNDO-FO3)} = 3.17eV - 2.94eV = 0.23eV$ compared to the low Stokes shift in PF of $E_{Stokes}^{PF} = 0.05eV$. The phonon energies, however, are close to those observed in absorption measurements in PF:

$$E_{ph,A,1}^{P(BiNDO-FO3)} = 3.39eV - 3.17eV = 0.22eV = 1747cm^{-1},$$
$$E_{ph,A,2}^{P(BiNDO-FO3)} = 3.59eV - 3.17eV = 0.42eV = 3410cm^{-1}.$$

As it was the case in PF the phonons coupled to the absorption spectrum are not the same as those coupled to the emission spectrum, and as in PF the third peak in the absorption spectrum is due to absorption of two phonons.

In the initial polyfluorenes such as BDOH-PF the blue emission were polluted by an unwanted green emission peak at $535nm$ $(2.32eV)$ turning the blue emitter in to a blue-green emitter. The EL spectrum in Fig. 4.18 was recorded from a device PF sandwiched between ITO and Ca/Al. The green emission can be a problem in e.g. full color displays where pure primary colors, i.e., red, green, and blue are required. The green emission peak was at first attributed to interchain excimer emission, where an excimer is a combined state due to interchain interaction between an excited state on one molecule and a ground state on another molecule. This was due to similar observations in LPPP attributed to excimers. Lately this assumption has been disproved by measurements indication the green emission to originate from keto defects, namely fluorenone[74, 75], where fluorenone is fluorene with oxygen instead of sidechains, see Fig. 4.19. The

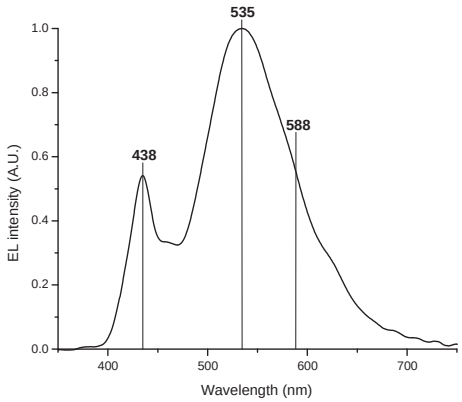

Fig. 4.18: The EL spectrum of PF polluted by unwanted green emission.

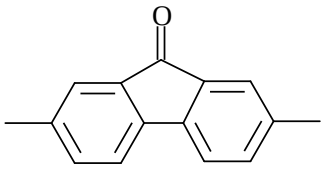

Fig. 4.19: The chemical structure of fluorenone.

main source of defects such as fluorenone is non-alkylated or only mono-alkylated monomers, that is fluorene monomers with none or only one alkyl side group attached. These not fully alkylated monomer act as centers for oxidation at any step in the synthesizing process. The fluorenone defect can also be formed after synthesis through oxidation of the polymer. The main argument against linking the green emission to excimer emission was the presence of green emission even in very dilute solutions[75]. In dilute solutions the molecules are separated making the intermolecular excimer formation impossible.

The peak at $588nm$ $(2.11eV)$ in the EL spectrum (Fig. 4.18) was found examining the negative second derivative of the spectrum. This peak is believed to be due to phonon coupling with the energy

$$E_{ph,E}^{PF*} = 2.32eV - 2.11eV = 0.21eV = 1684cm^{-1}.$$

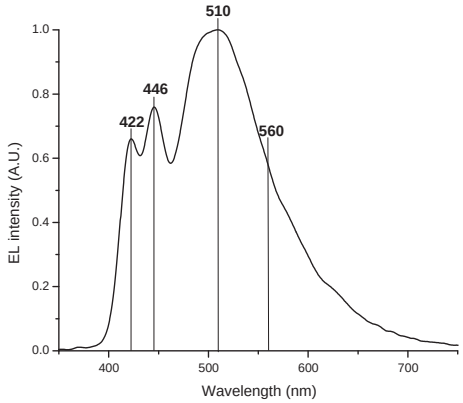

Fig. 4.20: The EL spectrum of P(BiNDO-FO3) polluted by unwanted green emission.

This phonon can be assigned to a carbonyl stretching mode, that is stretching of the C=O double bond[74], confirming the assumption that the green emission is due to fluorenone.

Scherf *et al.*[74] proposed that the defect states are not excited directly through electron hole capture but by Förster energy transfer from the PF backbone. However, Kulkarni *et al.*[75] found that electron-hole capture does occur in fluorenone and because the fluorenone act as a electron trap the efficiency of a green emitting fluorene/fluorenone device can be higher than a fluorene device. That is, the fluorenone defect is excited through both electron-hole capture and energy transfer from the PF backbone. Kulkarni *et al.* demonstrated that the use of fluorenone in low concentrations ($< 10\%$ of fluorene) will make the device an efficient green emitter with high electron injection because the presence of fluorenone lowers the electron injection barrier due to a higher electron affinity. In contrast to oxidation of PPV, the oxidation of PF does not quench the light emission but change the emissive properties of the polymer.

The emission from fluorenone was also observed in P(BiNDO-FO3) as Fig. 4.20 illustrates. The EL spectrum in Fig. 4.20 was recorded from a device with P(BiNDO-FO3) sandwiched between ITO and Ca/Al. However with a peak at $510nm$ ($2.43eV$) the emission has blue shifted with an energy increase of $0.11eV$ due to the conjugation breaking binaphthyl, just like the blue shift in emission from the PF backbone which also is blue shifted $0.11eV$ from $438nm$ to $422nm$. The second peak from green emission at $560nm$ (2.21eV) has been determined by examining the negative second derivative and with a phonon energy of

$$E_{ph,E}^{P(BiNDO-FO3)*} = 2.43eV - 2.21eV = 0.22eV = 1750cm^{-1},$$

it is assigned to a carbonyl stretching mode as in PF with fluoronene defects. It is

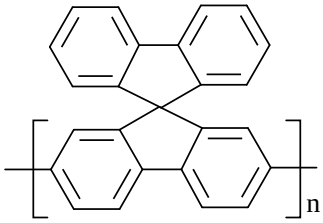

Fig. 4.21: The chemical structure of polyspirobifluorene.

noticeable that green emission was only observed in devices without PEDOT:PSS between ITO and the polymer. In other words, the ITO is a likely source for the oxygen involved in fluoronene generation. One candidate for pure blue emission without the unwanted green emission is polyspirobifluorene, see Fig. 4.21[76]. The fluorene monomer attached as sidegroup apparently prohibits fluorenone formation.

4.3 Phenylene Based Copolymers

The last group of conjugated polymers characterized here are the phenylene based copolymers. Different types of phenylene based copolymers, that is copolymers with phenylene as one of the two monomers in the copolymer chain and a variety of monomers as the second are investigated in terms of their PL and EL properties.

4.3.1 P(AnthBenzene)

One such copolymer is P(AnthBenzene) where the second monomer is anthracene. The polymer is synthesized via Suzuki coupling reaction of dibromoanthracene and a benzene diboronic acid and carefully purified. The synthesis scheme along with the chemical structure of the final copolymer is seen in Fig. 4.22. From a device with a layer P(AnthBenzene) spin coated from a $10\frac{mg}{ml}$ solution at $700RPM$ and sandwiched between a ITO/PEDOT-PSS anode and a Ca/Al cathode, the EL spectrum was recorded and plottet in Fig 4.23 along with a PL spectrum of a P(AnthBenzene) device. The PL measurements on the polymer was performed with an excitation wavelength of $361nm$ $(3.44eV)$ using the frequency doubled output from a mode-locked Ti-Sapphire laser. The first three peaks at $419nm$ $(2.96eV)$, $440nm$ $(2.82eV)$, and $485nm$ $(2.56eV)$ are observed primarily in PL, but can also be observed as peaks in the negative second derivative of the EL spectrum. The last three peaks at $523nm$ $(2.37eV)$, $586nm$ $(2.12eV)$,

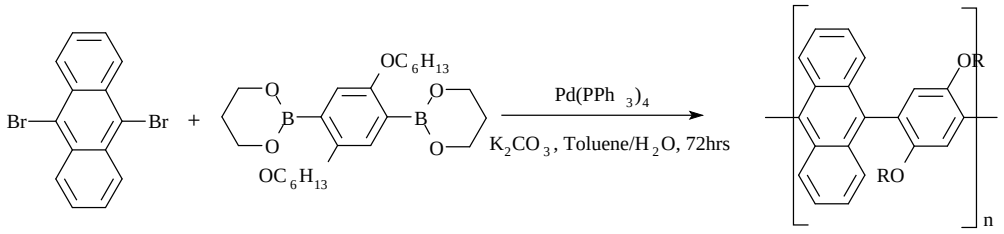

Fig. 4.22: The synthesis scheme of P(AnthBenzene).

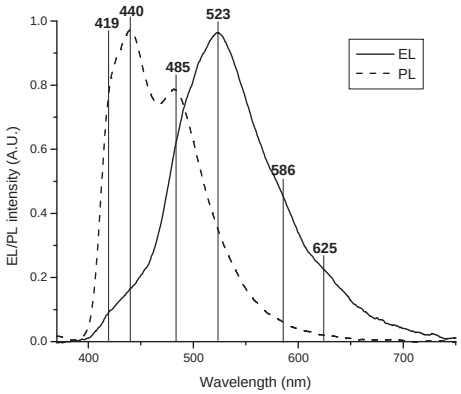

Fig. 4.23: The EL spectrum of a P(AnthBenzene) device and the PL spectrum of a P(AnthBenzene) device.

and $625nm$ $(1.98eV)$ are only observed in the EL spectrum or as peaks in the negative second derivative of the EL spectrum. The differences in the relative peak intensities between PL and EL are due to the difference in recombination zone in the two cases. In PL electron-hole pairs are generated throughout the device and therefore the recombination zone extends to the hole device. In EL, however, due to the low electron mobility the recombination zone is move to the electron injecting electrode, i.e. the metal electrode. The close proximity to the metal electrode affects the electron-phonon coupling and hereby change the relative intensities of the transitions. This difference between interface and bulk luminescence due to difference in electron-phonon coupling constants has also been observed in PPV[77, 78]. With the strong electron phonon coupling it is difficult to identify the phonons in the EL spectrum. The peaks in PL are due

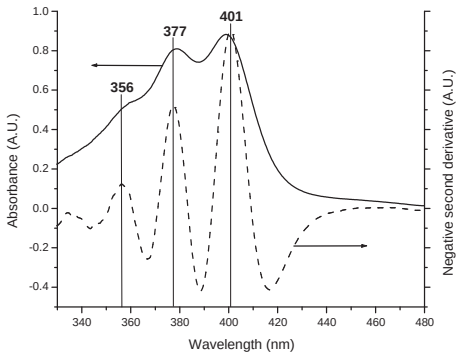

Fig. 4.24: The absorption spectrum and the negative second derivative of the absorption spectrum of P(AnthBenzene).

to phonons with energies:

$$E_{ph,E,1}^{P(AnthBenzene)} = 2.96eV - 2.82eV = 0.14eV = 1139cm^{-1},$$
$$E_{ph,E,2}^{P(AnthBenzene)} = 2.96eV - 2.56eV = 0.40eV = 3247cm^{-1}.$$

The two peaks are assigned to C-C and C-H stretching mode, respectively. The low intensity even in PL of the peak ($419nm$) without electron-phonon coupling (0-0) compared to the first peak ($440nm$) with electron-phonon coupling (0-1) is probably due to self-absorption, that is absorption of the emitted light by the polymer itself before it escapes the polymer.

Besides assigning the long wavelength peaks to strong electron-phonon coupling it is also a possibility that these peaks originate from excimer emission. Excimer emission has previously been observed from anthracene based molecules with green emission resembling what is observed in P(AnthBenzene)[79]. These molecules, however, still revealed emission at short wavelength with well resolved electron-phonon coupling peaks. These observations indicate that the green emission from the P(AnthBenzene) device is due to a combination of strong electron-phonon coupling, self-absorption and excimer emission.

The absorption spectrum of a thin P(AnthBenzene) film on a glass substrate has been measured and is illustrated in Fig. 4.24 along with the negative second derivative of the absorption spectrum which is included to identify the peak positions in the absorption spectrum. These peaks at $401nm$ ($3.09eV$), $377nm$ ($3.29eV$), and $356nm$ ($3.48eV$), however, are also directly identified in the absorption spectrum which was not the case in PPV or PF based polymers or copolymers. It was observed in P(AnthBenzene) because it has well resolved vibronic features which is common to anthracene containing polymers[80]. The Stokes shift in P(AnthBenzene) is $E_{Stokes}^{P(AnthBenzene)} = 3.09eV - 2.96eV = 0.13eV$,

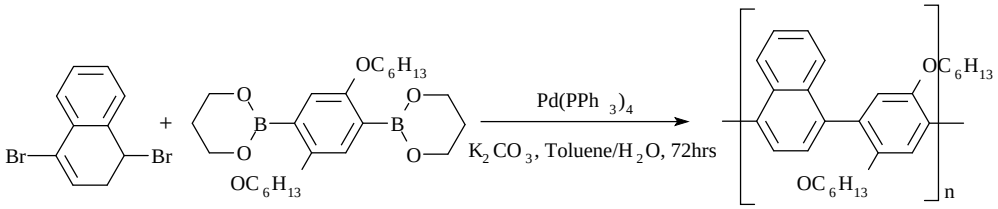

Fig. 4.25: The synthetic scheme of P(NaphBenzene).

i.e. it is larger than in PF but smaller than PPV. The phonon energies due to the electron-phonon coupling are:

$$E_{ph,A,1}^{P(AnthBenzene)} = 3.29eV - 3.09eV = 0.20eV = 1588cm^{-1},$$
$$E_{ph,A,2}^{P(AnthBenzene)} = 3.48eV - 3.09eV = 0.39eV = 3152cm^{-1}.$$

The second energy $E_{ph,A,2}^{P(AnthBenzene)}$ is the double of $E_{ph,A,1}^{P(AnthBenzene)}$, that is, the peak at $356nm$ is due to electron coupling to two phonons. The absorption spectrum confirms the possibility of self-absorption of the $419nm$ emission peak because the absorption peak at $401nm$ extends beyond $420nm$. The results presented here, regarding absorption and PL spectrum, and the Stokes shift is in agreement with result on a similar polymer presented by Kaeriyama *et al.*[81]. In the work by Hirohata *et al.* a copolymer resembling P(AnthBenzene), but with an ethynylene group, that is a triple bond and a single bond, between every anthracene and benzene monomer. The EL spectrum of this polymer sandwiched between Al and ITO showed similar broad excimer emission, though red-shifted compared to P(AnthBenzene) resulting in red emission with peak at $590nm$. In another device based on a polymer with phenylene and anthracene in the backbone blue emission was achieved[82]. In other words phenyleneanthracene based devices are capable of achieving emission in a broad range by modifications of the backbone.

4.3.2 P(NaphBenzene)

Another phenylene based copolymer is P(NaphBenzene) with naphthalene as the second monomer in the polymer chain. The polymer is synthesized via Suzuki coupling reaction of dibromonaphthelene and diboronic acid and purified. The chemical structure of the final copolymer and the synthetic scheme is seen in Fig. 4.25. From a device with a P(NaphBenzene) layer spin coated from a $10\frac{mg}{ml}$ solution at $700RPM$ and sandwiched between a ITO/PEDOT-PSS anode and a Ca/Al cathode, the EL spectrum was recorded and plottet in Fig 4.26 along

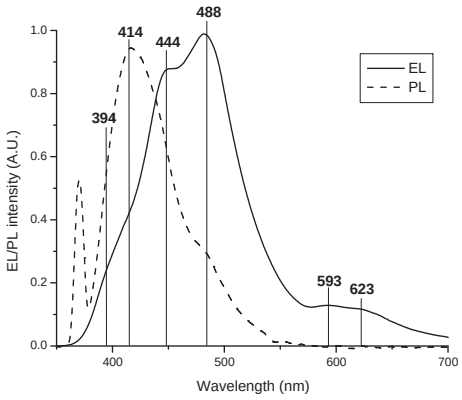

Fig. 4.26: The EL spectrum of a P(NaphBenzene) device and the PL spectrum of a P(NaphBenzene) device.

with a PL spectrum of a P(NaphBenzene) device. The PL measurements on the polymer was performed with an excitation wavelength of $370nm$ $(3.35eV)$ using the frequency doubled output from a mode-locked Ti-Sapphire laser. The excitation wavelength is seen as the first peak in the PL spectrum. As it was the case in P(AnthBenzene) there is a strong electron-phonon coupling at the metal-polymer interface resulting in a shift in the relative intensities of the peaks between PL and EL. The long wavelength peaks at $593nm$ and $623nm$ are due to excimer emission . The first three peaks identified in the negative second derivative of both PL and EL are located at $394nm$ $(3.15eV)$, $414nm$ $(3.00eV)$, and $444nm$ $(2.79eV)$. The two latter peaks are due to electron-phonon coupling with phonons having the energies:

$$E_{ph,E,1}^{P(NaphBenzene)} = 3.15eV - 3.00eV = 0.15eV = 1226cm^{-1},$$
$$E_{ph,E,2}^{P(NaphBenzene)} = 3.15eV - 2.79eV = 0.35eV = 2958cm^{-1}.$$

As in P(AnthBenzene) these phonons are assigned to C-C and C-H stretching mode, respectively.

The absorption spectrum of a thin P(NaphBenzene) film on a glass substrate have been measured and is illustrated in Fig. 4.27 along with the negative second derivative of the absorption spectrum which is included to identify the peak positions in the absorption spectrum. With peaks at $346nm$ $(3.58eV)$ and $322nm$ $(3.85eV)$ the Stokes shift $E_{Stokes}^{P(NaphBenzene)} = 3.58eV - 3.15eV = 0.43eV$ is rather large. The phonon coupled to the electron transition in the absorption measurements has the energy:

$$E_{ph,A,1}^{P(NaphBenzene)} = 3.85eV - 3.58eV = 0.27eV = 2154cm^{-1},$$

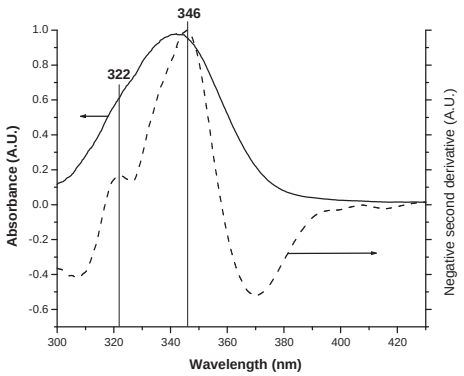

Fig. 4.27: The absorption spectrum and the negative second derivative of the absorption spectrum of P(NaphBenzene).

which is difficult to link to a specific phonon mode. The lower emission intensity in the PL spectrum of the 0-0 transition at $394nm$ compared to the 0-1 transition at $414nm$ is due to strong electron-phonon coupling even in the bulk of the polymer. It cannot be assigned to self-absorption because the large Stokes shift means there is no overlap between the emission and the absorption spectrum, which is necessary in self-absorption.

A polymer like P(NaphBenzene), but with a vinylene group, i.e. a single and a double bond, between every naphthalene and benzene monomer was synthesized by Sun *et al.*[83]. The absorption and luminescence measurements on this polymer showed similar properties, i.e. large Stokes shift and significant difference between PL and EL spectrum. All measurements, however, was red shifted due to the presence of the vinylene group in the backbone. As it was the case for P(NaphBenzene), the difference between PL and EL spectrum was assigned to strong electron-phonon coupling and excimer emission. Similar results was achieved with a carbazole and nathalene based copolymer, i.e. large Stokes shift and difference between PL and EL spectrum, though all measurements where again significantly red-shifted except for the excimer emission which match was is observed in P(NaphBenzene)[84]. That is, it seems reasonable to assign these properties to the presence of naphthalene in the backbones of the polymers.

4.3.3 P(BiNaphBenzene)

The last phenylene based copolymer investigated here is P(BiNaphBenzene) where the second monomer in the polymer chain is binaphthalene. The polymer is synthesized via Suzuki coupling reaction of a binaphthyl dibromide and diphenylboronic acid and carefully purified. The synthetic scheme and the chemical struc-

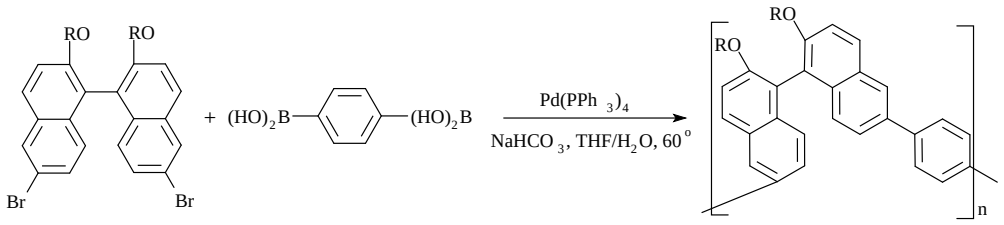

Fig. 4.28: The synthetic scheme of P(BiNaphBenzene).

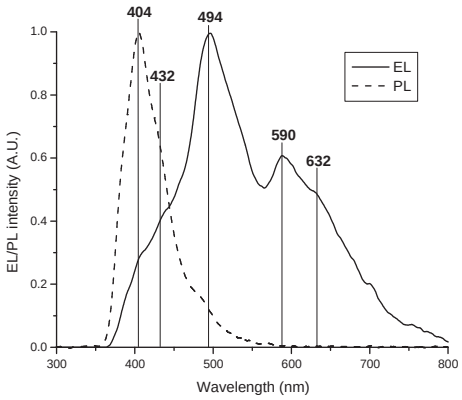

Fig. 4.29: The EL spectrum of a P(BiNaphBenzene) device and the PL spectrum of a P(BiNaphBenzene) device.

ture of the final copolymer is depicted in Fig. 4.28. From a device with a layer of P(BiNaphBenzene) spun from a $10\frac{mg}{ml}$ solution at $700RPM$ and sandwiched between a ITO/PEDOT-PSS anode and a Ca/Al cathode, the EL spectrum was recorded and plottet in Fig 4.29 along with a PL spectrum of a P(NaphBenzene) device. The PL measurements on the polymer was performed with an excitation wavelength of $340nm$ $(3.65eV)$ using the frequency doubled output from a Nd:YAG laser. Once more the strong electron-phonon coupling in the EL result in a large shift in the relative intensities of the peaks between PL and EL. With peaks at $404nm$ $(3.07eV)$ and $432nm$ $(2.87eV)$ found in both EL and PL by picking peaks in the negative second derivatives of the two, the phonon energy involved in the transition resulting in the $432nm$ peak is

$$E_{ph,E,1}^{P(BiNaphBenzene)} = 3.07eV - 2.87eV = 0.20eV = 1604cm^{-1}.$$

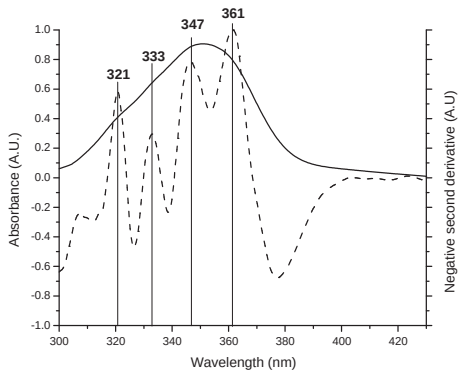

Fig. 4.30: The absorption spectrum and the negative second derivative of the absorption spectrum of P(BiNaphBenzene).

The long wavelength peaks at $590nm$ and $632nm$ are due to excimer emission as it was the case in P(NaphBenzene). The positions of the peaks are close to those observed in P(NaphBenzene), but the intensities of these peaks compared to the non-excimer emission peaks are much higher in P(BiNaphBenzene) because of stronger interchain coupling resulting in excimer emission.

The absorption spectrum of a thin P(BiNaphBenzene) film on a glass substrate has been measured and is illustrated in Fig. 4.30 along with the negative second derivative of the absorption spectrum, which is included to identify the peak positions in the absorption spectrum. These peaks are positioned at $361nm$ $(3.44eV)$, $347nm$ $(3.57eV)$, $333nm$ $(3.72eV)$, and $321nm$ $(3.86eV)$ again giving a large Stokes shift as in P(NaphBenzene) of $E_{Stokes}^{P(BiNaphBenzene)} = 3.44eV - 3.07eV = 0.37eV$. With four peaks the three phonon energies are

$$E_{ph,A,1}^{P(BiNaphBenzene)} = 3.57eV - 3.44eV = 0.13eV = 1118cm^{-1},$$
$$E_{ph,A,2}^{P(BiNaphBenzene)} = 3.72eV - 3.44eV = 0.28eV = 2329cm^{-1},$$
$$E_{ph,A,3}^{P(BiNaphBenzene)} = 3.86eV - 3.44eV = 0.42eV = 3452cm^{-1}.$$

The first phonon $E_{ph,A,1}^{P(BiNaphBenzene)}$ is due to a C-C stretching mode, and the second $E_{ph,A,2}^{P(BiNaphBenzene)}$ and the third $E_{ph,A,3}^{P(BiNaphBenzene)}$ is double and triple of the first, that is the peaks at $333nm$ and $321nm$ is probably due to coupling to two and three phonons, respectively. Other binaphthyl based polymers such as polymers based on pure binaphthyl[85] and copolymers with binaphthyl and phenylene vinylene monomers[72] have similar optical properties, i.e. large Stokes shifts and strong electron-phonon coupling and excimer emission resulting in significant differences between PL and EL spectra. The lowering of the EL efficiency

due to the the conjugation breaking binaphthyl seen in P(BiNDO-FO) was not observed in P(BiNaphBenzene).

4.4 Conclusion

In this chapter a number of polymers have been investigated resulting in PLED devices having EL in the entire visible range. The first branch of polymers considered were the PPVs which also was the first CP to give EL. Main focus was put on the PPV derivative MEH-PPV, which was the first soluble PPV derivative to show EL. MEH-PPV has red emission with peak at $587nm$ and electron-phonon coupling giving a peak at $640nm$. The polymer has a significant Stokes shift resulting in absorption with electron-phonon coupling below $525nm$. The IV-characteristics on a MEH-PPV device was also measured revealing a device with nice diode behavior, traps in the polymer and a critical voltage above which the traps are filled of $3V$. Four copolymers with phenanthroline and phenylene vinylene monomers and different side groups to the two monomers was synthesized and characterized with PL and EL was recorded from one of the four. The sidegroup to the phenanthroline was either H or phenyl with a blue shift in PL emission in the former compared to the latter. The side group of the phenylene vinylene did not change the emission peak positions but the larger of the two side groups lead to an increased electron-phonon coupling compared with the smaller of the two side groups resulting in a shift in peak intensities of the different transitions. The second branch of polymers investigated was the polyfluorenes and fluorene containing copolymers. The polyfluorenes based polymer are blue emitting polymers with the primary peak at $440nm$ and below. The polyfluorenes based polymers have well resolved vibronic features in the emission spectrum because of the more rigid structure reducing the vibrations from torsion of the phenylene ring which are responsible for broadening. The copolymers have been synthesized with fluorene and binaphthyl monomers in 1:1 P(BiNDO-FO) and 3:1 P(BiNDO-FO3) ratio. The purpose of this was to use the binaphthyl monomer which has large dihedral angle between the two naphthyl groups as a conjugation breaker, and this way synthesize polymers with short conjugation lengths of one and three fluorene monomers in P(BiNDO-FO) and P(BiNDO-FO3), respectively. The result of the short conjugation lengths are a blue shift in emission between PF and P(BiNDO-FO3) and between P(BiNDO-FO) as well. Defects due to oxidation of PF and P(BiNDO-FO3) was also observed, however unlike PPV these defects did not lead to quenching of the emission, but rather to green emission at $535nm$ in PF. The green emission, however, can also pose a problem if pure blue emission is desired, e.g. in a display. Phonon modes were observed in the green emission which could be assigned to carbonyl stretching confirming the origin of the green emission to oxygen defects (fluorenone), in contrast to early theories which assigned it to excimer emission. As mentioned the green fluorenone emission was

also observed in P(BiNDO-FO3) and again with a phonon which could be assigned to carbonyl stretchin, however blue shifted to $510nm$ which is a blue shift $0.11eV$, just like the blue shift of the blue emission due to the shorter conjugation lengths. The green fluorenone emission was only observed in devices without PEDOT:PSS between ITO and the polymers. This makes ITO a likely source for the oxygen needed for fluorenone formation. The third and final branch of conjugated polymers was the phenylene based copolymers, that is copolymers where phenylene is one of the two monomers in the polymer chain. The first of these copolymers are P(AnthBenzene), which have anthracene as the second monomer. Devices based on P(AnthBenzene) showed a large shift in the relative intensities of the peaks between the PL and the EL spectrum which was attributed to stronger electron-phonon coupling at the metal polymer interface where electron and holes recombine is in case of EL than in the bulk which is where electron and holes recombine in PL. Furthermore new peaks appeared in the EL spectrum due to excimer emission. The intensity of the peak originating from the electronic transition which is not coupled to a phonon is lower than the first peak originating from a phonon coupled electronic transition even in PL, which is unusual. This is due to the strong electron-phonon coupling and self-absorption, the latter being possible because of the relatively low Stokes shift in P(AnthBenzene). The other two phenylene based copolymers are P(NaphBenzene) and P(BiNaphBenzene) with naphthyl and binaphthyl monomer in the polymer chain, respectively. They both have a strong electron-phonon coupling at the metal-polymer interface and excimer emission which is the cause of a large difference between PL and EL spectrum. The excimer emission was more pronounced in P(BiNaphBenzene) due to a stronger interchain coupling which is the source of the excimer emission. A lowering of the first peak in the PL spectrum was observed in P(NaphBenzene) but not in P(BiNaphBenzene). The lowering of the peak in P(NaphBenzene) was purely due to electron-phonon coupling because a large Stokes shift in both polymers means self-absorption is impossible.

Chapter 5

Energy Transfer

A huge driving force behind the research in PLEDs is the prospect of producing displays based on PLEDs. PLEDs usually have a broad emission band due to vibration states and inhomogeneous broadning. This possesses a problem since sharp emission bands are necessary to produce the pure colors needed in displays. Especially red emission has been problematic as the eye is more sensitive to orange than to red emission resulting in the red emitter appearing orange even at low intensities of orange emission. The results presented in this chapter have been published in Ref. [2].

5.1 Introduction

There are several different approaches to achieve red emission, one of which is to apply a filter on top of the device to remove the unwanted orange emission. The drawback of this approach, however, is that it leads to a reduced efficiency of the device because it removes a part of the luminescence. Furthermore the addition of a filter to the device would add one or more extra steps in the production of PLEDs, which is obviously undesirable if it where to be commercialized. Another approach is to red-shift the emission spectrum of the polymer or introduces red-emitting organic chromophores, that is small organic molecules with high PL efficiency, which are excited through Förster energy transfer. The red-shift in the emission spectrum could be achieved by incorporating low bandgap thiophene monomers in a fluorene based copolymer[86], where thiophene is an aromatic ring with four carbon atoms and one sulfur atom. The emission spectrum in both cases, however, still reveals broad emission bands and the red shift required to make the emission appear red means, a significant portion of the emission is outside the visible range or at least in a range where the eye has low sensitivity, which lowers the efficiency of the device. It was demonstrated by Baldo *et al.* that relatively narrow band red emission could be achieved through doping of Alq_3

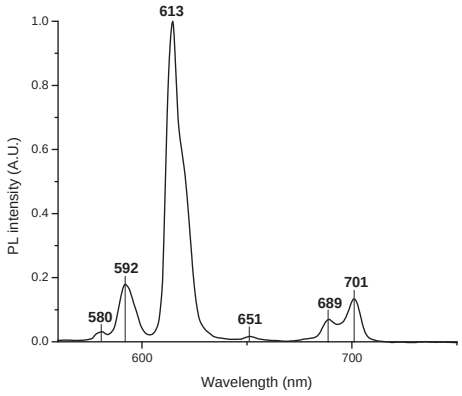

Fig. 5.1: The emission spectrum of the Eu(dnm)$_3$phen complex.

with a platinum containing phosphorescent dye[52]. It was necessary with high concentration of the dye to achieve complete energy transfer from the Alq_3. This leads to the conclusion that the dye was excited through Dexter energy transfer because this transfer mechanism has short range, i.e. high concentration of the acceptor molecule was needed to get short distances between donor and acceptor leading to efficient Dexter energy transfer. It was found, however, that as the current was increased the emission shifted towards orange because of saturation in the Dexter energy transfer. Saturation in the Dexter energy transfer is possible due to the long lifetime of the platinum containing phosphorescent dye. Doping a polymer with nanocrystals of a cyanine dye has also been found to lead to narrow band red emission[87]. The purpose of the dopant in this case, however, was not to act as acceptor in a energy transfer process but to lower to bandgap to achieve red emission.

5.2 Eu Complexes

The approach investigated here is to use a europium complex to achieve red emission since it has a high photoluminescence efficiency and a sharp emission spectrum at the desired wavelength[88]. The PL spectrum of a europium complex have been recorded and is illustrated in Fig. 5.1. The PL spectrum is recorded with an excitation wavelength of $385nm$ using the frequency doubled output from a mode-locked Ti-Sapphire laser. The excitation process of the Eu ion in the complex occurs as follows. The ligand is excited to a singlet exciton which through a intersystem crossing turns into a triplet exciton that transfers energy

Wavelength	Transition
$580nm$	$^5D_0 \rightarrow ^7F_0$
$592nm$	$^5D_0 \rightarrow ^7F_1$
$613nm$	$^5D_0 \rightarrow ^7F_2$
$651nm$	$^5D_0 \rightarrow ^7F_3$
$689nm$	$^5D_0 \rightarrow ^7F_4$
$701nm$	$^5D_0 \rightarrow ^7F_4$

Table 5.1: The transitions involved in emission in a Eu ion[67].

to the Eu ion. The direct energy transfer from the singlet state has been found to be insignificant[89]. That is, the ligands act as antennas which absorbs energy and transfer it to the Eu ion. In order to transfer energy to the Eu ion, the triplet level has to be above the emissive $^5D_0$-level and the absorption of the complex is thus blue shifted by at least the exchange energy of the ligand compared to the $^5D_0$-level of the Eu ion. Eu complexes has absorption peaks at approximately 400nm, depending on the conjugation length of the ligand[90], and is known to have long PL lifetime, i.e. above $100\mu s$[67]. As it is observed in Fig. 5.1 the europium ion has a very dominant peak at $613nm$ making it appear red emitting and a few peak at both higher and lower wavelength which are to faint to pollute the red emission. The peaks are assigned to different transitions given in Table 5.1 The peak at $613nm$ peak in the Eu complex is very sharp (FWHM$< 10nm$) as it is observed in Fig. 5.1, unlike the polymers or organic chromophores. The dominating $^5D_0 \rightarrow ^7F_2$ transition is know to be very sensitive to the surrounding environment[91]. The intensity decreases in symmetric environment which the PL measurements (Fig. 5.1) indicate is not the case in the Eu complex. The Eu complex with the described PL emission properties is Eu(dnm)$_3$phen and has the chemical structure illustrated in Fig. 5.2. Other complexes based on trivalent rare earths, such as terbium and erbium, share these properties of high photoluminescence efficiency and sharp emission spectrum[92, 93].

5.3 Eu Complexes in Devices

Several different approaches have been used to benefit from the desirable luminescence properties of Eu complexes. One approach is to use a Eu complex directly as emitting layer. This has been done with different hole- and electron transport layers[94, 95]. EL can also be achieved from a device with pure Eu complex, however, only with low luminance because of the low carrier mobility and concentration quenching in the Eu complex. The purpose of the hole- and electron

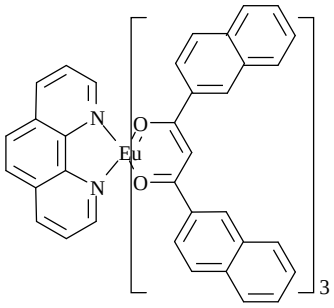

Fig. 5.2: The chemical structure of the Eu(dnm)$_3$phen complex.

transport layers is thus to increase the mobility of the charges and hereby increase the luminance. Codeposition of the Eu complex with a electron transport layer can increase the efficiency of a device because concentration quenching is avoided. The codeposition also leads to better film forming and increased luminance due to increased mobility of the emitter layer.

Another approach is to attach the Eu complex to the backbone of a light emitting polymer and through intramolecular Förster energy transfer obtain light emission from the Eu complex. As described in Sec. 2.5.2 regarding Förster transfer there has to be an spectral overlap between the absorption spectrum of the Eu complex and the emission spectrum of the donor, and because the ligands absorb at approximately $400nm$ the donor has to be a blue emitter such as the fluorene based polymer mentioned in Sec. 4.2. The Förster energy transfer could be achieved by attaching bipyridyl as a side group to fluorene based polymer, with bipyridyl being two aromatic ring with five carbon atoms and one nitrogen atom in each ring[96, 67]. The bipyridyl side group replaces the phenanthroline in the Eu complex, i.e. the part of the complex to the left of Eu-ion in Fig. 5.2. The energy is transferred from the backbone of the polymer to ligand of the attached Eu complex by intramolecular Förster energy transfer and then to the Eu ion as described in Sec. 5.2. It was found by Pei *et al.*[96] that the attachment of the Eu complex to the backbone of the polymer does not change the energy levels in the polymer. Attaching both the blue emitting donor and the acceptor, i.e. the Eu complex, in the Förster energy transfer process, to the polymer backbone has also been demonstrated, however with less success[97].

Finally one can make a blend of a light emitting polymer and a Eu complex and through intermolecular Förster energy transfer get light emission from the Eu complex. One advantage of this approach is the possibility to spin the donor polymer used in the Förster energy transfer and applied the acceptor such as a Eu complex where the red emission is desired. This way it is possible to

effectively write the pixels in a polymer display. The technique has been proven by McGehee *et al.*[90] who found that with the right solvent the spin coated polymer could be desolved locally and the dopant would defuse into the polymer. Again the spectral overlap between the emission spectrum of the polymer and the absorption spectrum of the Eu complex is of great importance. Therefore, a polymer is needed with emission peak as close to 400nm as possible where the absorption in Eu complexes occurs. However, conjugated polymers usually have emission at longer wavelengths. Thus, to achieve most efficient energy transfer one should choose the polymer with emission peaks at the shortest wavelengths and a Eu complexes with absorption at the longest wavelengths. There have been reports of successful doping of different polymers and organic molecules such as cyano substituted PPP[90] and carbazole based polymers[90, 98] and carbazole based organic molecules[99]. Polyfluorene containing binaphtyl has been demonstrated as an efficient blue-emitter which are described in Sec. 4.2 where it was also demonstrated how the incorporation of conjugation breaking binaphthyl blue-shifted the emission spectrum, which will increase the overlap with the absorption spectrum of the Eu complex. It will be demonstrated here that blending this polymer with a Eu complex makes it possible to achieve red emission, through intermolecular Förster energy transfer from the blue-emitting polymer to the Eu complex. PF has been used in a blend with the same Eu complex, resulting in no energy transfer and hence no red emission.

A blend of Eu(dnm)$_3$phen complex and Poly(9,9-dioctylfluorenyl-2,7-diyl), PF and Poly[(6,6'-(2,2'-didodecyloxyl)-1,1'-binaphtyl)-co-(9,9'dioctylfluorene)] (25:75 in moles), P(BiNDO-FO3) was disolved in THF to demonstrate energy transfer from polymer to Eu complex. The Eu(dnm)$_3$phen complex and the PF polymer were purchased from American Dye Source, Inc. whereas P(BiNDO-FO3) was synthesized as described in Sec. 4.2. The absorption spectrum of a thin Eu complex film on a glass substrate was recorded and plottet in Fig. 5.3 along with the emission spectrum of PF and P(BiNDO-FO3) previously recorded in order to assess the spectral overlap between absorption of the Eu complex and emission of the two polymers. It is observed that there is only a small spectral overlap between the absorption in the Eu complex and the emission from P(BiNDO-FO3) and there is no spectral overlap between the Eu complex and PF.

Single-layer devices were fabricated with a ITO/Polymer:Eu(dnm)$_3$phen/Ca/Al structure. ITO coated glass substrates was cleaned by ultrasonication in acetone, demineralized water and ethanol and then blow dried. The Eu complex was blend into the polymer solution at a 20 wt.-%. The polymers were spincoated onto the substrates from a THF solution, PF with Eu complex from a $6\frac{\text{mg}}{\text{ml}}$ solution spun at 1500RPM and P(BiNDO-FO3) with and without Eu complex from a $12\frac{\text{mg}}{\text{ml}}$ solution spun at 700RPM. The polymer layers are in all cases approximately 100nm thick. Al was evaporated on top of the Ca cathode to protect the Ca from oxidation. Ca and Al were thermally evaporated at a base pressure of $\sim 10^{-6}$mbar and with a deposition rate of $1.0\frac{\text{nm}}{\text{s}}$ and $0.5\frac{\text{nm}}{\text{s}}$, respectively, and with a thickness of

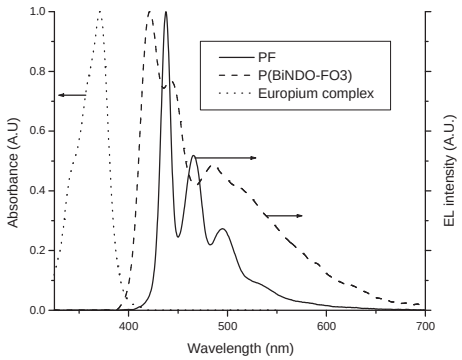

Fig. 5.3: Absorption spectrum of the Eu complex, and emission spectrum of the two host polymers, PF and P(BiNDO-FO3).

70nm and 130nm, respectively. Both metals were evaporated through a circular shadow mask with a larger diameter in case of the Al to ensure encapsulation of the Ca. The devices have an emitting area of approximately 30mm^2. Device fabrication and experiments where performed at room temperature and in ambient atmosphere.

While operating the devices in continuous DC mode with the ITO biased positively the EL spectrum was recorded. The EL spectrum of devices with P(BiNDO-FO3), shown in Fig. 5.4, has peaks at 422nm, 445nm and 485nm, whereas the EL spectrum of PF, shown in Fig. 5.5, has peaks at 438nm, 466nm and 495nm confirming the results of previous recorded on both polymers. As mentioned earlier this blue-shift from PF to P(BiNDO-FO3) is quite significant since it is towards the absorption peak of the Eu complex. For this reason a peak at 613nm was observe in P(BiNDO-FO3):Eu(dnm)$_3$phen complex blends and not in PF:Eu(dnm)$_3$phen complex blends. From these observations it can be concluded that energy transfer is possible from P(BiNDO-FO3) although it is not very efficient in this blend. In the investigations by McGehee *et al.* it was found that the absorption spectrum of the polymer was identical to the blend, that is the absorption was unaffected by the addition of Eu complex which indicate that only the polymer absorbs and the subsequently transfer energy to the Eu complex. Similar observations was made for the P(BiNDO-FO3):Eu(dnm)$_3$phen complex blend. Due to the inefficiency of the energy transfer pure red emission was not achieved, because the blue emission from the host polymer was still dominant. The inefficient energy transfer is caused by a small spectral overlap between the emission in the polymer and absorption in the Eu complex which was also observed in Fig. 5.3. Replacing phenanthroline in the Eu complex with Michler's ketone (MK) as described by Werts *et al.*[100] which leads to a red-

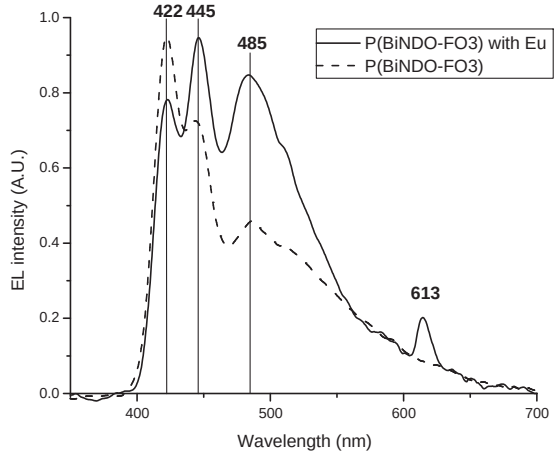

Fig. 5.4: Electroluminescence from P(BiNDO-FO3) with Eu complex (full line) and without Eu complex (dotted line)

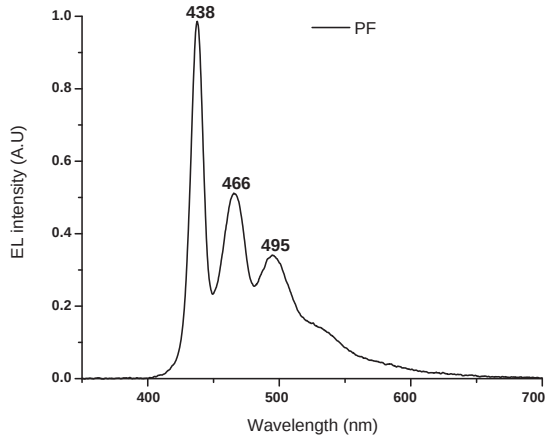

Fig. 5.5: Electroluminescence from PF blend with Eu complex, showing no energy transfer

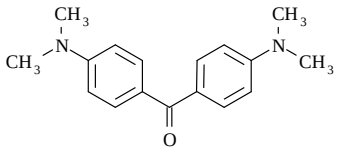

Fig. 5.6: The chemical structure of Michler's ketone.

shift in the absorption spectrum could be a possible solution, with the chemical structure of MK illustrated in Fig. 5.6. The Eu complex developed by Werts *et al.* has maximum absorption at 414nm which would lead to a stronger overlap with the primary peak in P(BiNDO-FO3) compared with the $Eu(dnm)_3phen$ used here. The source of the red-shift in absorption is a lowering in the singlet energy level responsible for absorption in the ligand, but without a lowering in the triplet level responsible for the energy transfer to the emissive $^5D_0$ level in the Eu ion, i.e. the triplet level is still high enough to transfer energy to the Eu ion, that is above the $^5D_0$ level at $2.14eV$ ($580nm$). The exchange energy is thus significantly reduced by the addition of MK to the Eu complex. This improvement upon incorporation of MK was expected because ketones are known to have small exchange energies[92]. It is noticeable that the addition of Eu complex does not change the position of the peaks originating from polymer. However, the relative intensities of these peaks change, indicating strongest absorption of the primary peak at 422nm in P(BiNDO-FO3) as expected whereas there is no change in the relative intensities in PF, because there is no spectral overlap.

There has been several reports of increased efficiency in polymers doped with a Eu complex compared to the undoped polymer[90, 99]. This was assigned to trapping of charges by the Eu complex which increases the probability of electron-hole capture to form an exciton as opposed to the situation where charges drift through the polymer layer without exciton formation. Blending a rare earth complex with a polymer to achieve light emission from the rare earth ion through Förster energy transfer has also been demonstrated with other rare earths such as terbium[92] and erbium[93]. These two rare earth ions both have strong emission at $545nm$ ($2.27eV$) which can be used as green emitter in a display and erbium also has infrared emission at $1.54\mu m$ ($0.81eV$) which can be used for optical communication, because optical fibers has very low loss at this wavelength. The emission properties of the rare earth ions is generally independent of the ligands because the energy levels responsible for emission is shielded against interaction with the ligands by outer shells in the rare earth ion. The purpose of the ligands is thus only to absorb light and subsequently transfer the energy to the rare earth ion.

5.4 Conclusion

In this chapter different approaches to achieve red emission to be used in e.g. display have been considered. It has been found that an efficient red emitting device has to have a sharp emission peak because of the low sensitivity of the eye towards red light. Sharp emission peaks are hard to achieve from polymers because of electron-phonon coupling and inhomogeneous broadening result in broad emission. Rare earth ions on the other hand are known to have sharp emission peaks and Eu ion has emission peak in the red part of the spectrum making it an obvious candidate for red emission. Eu complexes, that is small organic molecules with a Eu ion in the middle, have been used in different devices where the complexes are excited either directly or through intra- or intermolecular Förster transfer. Intermolecular Förster energy transfer from a polyfluorene based polymer to a Eu complex has been demonstrated. However, the energy transfer is not efficient enough to achieve pure red emission. This could probably be solved by using a Eu complex with a red-shifted absorption spectrum. The absorption spectrum of the Eu complex depends primarily on the ligands because the central Eu ion responsible for the emission properties is excited through a process involving absorption by the ligand generating a singlet exciton on the ligand, intersystem crossing of the exciton to a triplet, and subsequent energy transfer to the Eu ion. The importance of using polyfluorene containing binaphthyl rather than pure polyfluorene was demonstrated, since the latter show no energy transfer. This is due to the blue-shift in emission from the polymer upon introduction of the conjugation breaking binaphthyl monomer described in Chap. 4. As a result of the blue-shift, the P(BiNDO-FO3) has spectral overlap between emission of the polymer and absorption of the Eu complex, which PF and Eu complex does not.

Part III

Contact Electrodes

Chapter 6

Characterizing Contact Electrodes

The importance of characterizing the contact materials is clear due to the effect of these on device efficiency through e.g. charge injection and device lifetime, the latter which can be reduced by defects due to oxidation by ITO. The main focus here, however, will be on determination the workfunctions of the contact materials because of the great influence of these on the charge injection.

6.1 Introduction

When fabricating polymer devices with the polymer sandwiched between a high workfunction anode and low workfunction cathode to improve charge injection, the difference in workfunction induces a built-in electric field. That is, there is an internal electric field in the device even without an external applied electric field. The source of this built-in electric field is the rearrangement of charges between polymer/cathode and polymer/anode interfaces due to the difference in workfunctions between the two contacts. That is, due to Fermi level alignment electrons are transferred from the low workfunction cathode to the high workfunction anode as illustrated in Fig. 6.1. If there is no build up of charges in the polymer due to defects and if the workfunctions of the contacts both are between HOMO and LUMO of the polymer the built-in electric field is uniform and given by[101]:

$$E_{Bi} = \frac{V_{Bi}}{L},$$

where L is the thickness of the device and V_{Bi} is the built-in voltage given by:

$$V_{Bi} = \frac{\Phi_a - \Phi_c}{e},$$

with e being the elementary charge and Φ_a and Φ_c are the workfunctions of the anode and cathode, respectively. The upper limit of the built-in electric field in

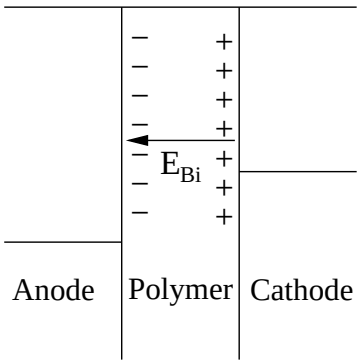

Fig. 6.1: Charges are rearranged in the polymer due to the contacts in a device.

a device is the energy gap of the polymer, that is the built-in electric field only scales with the difference of the workfunction if it is below this limit[102].

6.2 Electroabsorption

Different methods have been applied to determine the built-in electric field in devices. Among these are electroabsorption which utilizes the change in absorption due to an applied alternating electric field. The change in absorption due to the applied alternating electric field is related to the third-order susceptibility $\chi^{(3)}$ and the squared electric field E [103]:

$$EA = \frac{-\Delta T}{T} \propto \mathrm{Im}\chi^{(3)} E^2, \tag{6.1}$$

with T being the transmission. If the electric field are composed of both dc and ac electric fields as well as the built-in electric field the total electric field is:

$$E = E_{dc} + E_{ac}\cos(\omega t) - E_{Bi}, \tag{6.2}$$

where E_{dc} is the applied electric dc field, E_{ac} is the amplitude and ω is the frequency of the applied electric ac field. The built-in electric field is subtracted because the applied electric field is positive, when the anode is biased positively, that is, the applied and the built-in electric fields are opposite. Inserting (6.2) in

to (6.1) gives

$$\begin{aligned} EA &\propto \mathrm{Im}\chi^{(3)}\left(E_{dc}+E_{ac}\cos(\omega t)-E_{Bi}\right)^2, \\ &\propto \mathrm{Im}\chi^{(3)}((E_{dc}-E_{Bi})^2+2(E_{dc}-E_{Bi})E_{ac}\cos(\omega t) \\ &\quad +E_{ac}^2\cos^2(\omega t)), \\ &\propto \mathrm{Im}\chi^{(3)}((E_{dc}-E_{Bi})^2+2(E_{dc}-E_{Bi})E_{ac}\cos(\omega t) \\ &\quad +E_{ac}^2\frac{\cos(2\omega t)+1}{2}). \end{aligned} \tag{6.3}$$

From (6.3) it is observed that the electroabsorption response can be divided in to a dc response, an ac response with the same frequency as the applied ac electric field, and an ac response with double the frequency. The ac response with the same frequency as the applied ac electric field is

$$EA(\omega) \propto 2(E_{dc}-E_{Bi})E_{ac}\cos(\omega t),$$

and is immediately observed that the built-in electric field can be determined as the applied electric dc field which cancels out the same frequency ac response of electroabsorption. The electroabsorption also has a wavelength dependence of the probe light through the third-order susceptibility, but the built-in field is determined at a constant wavelength. This technique has been applied on a number of different PPV based devices with different contacts in order to determine the built-in fields[104, 103, 101, 102]. The results of these experiments confirms that the built-in electric field indeed is determined by the difference in workfunctions between the two contacts and that the polymer between the contacts sets the upper limit for the built-in electric field.

Other methods to determine the built-in field has been developed such as saturated photovoltage. The photovoltage, also termed the open-circuit voltage, is the voltage across a device under illumination, that is the device is operated as a solar cell. The photovoltage scales with logarithmically with illumination until it saturates at the built-in voltage[105].

6.3 Electric Field Induced Second Harmonic Generation

In this section another method for determining the built-in field will be developed. This method is based on the second harmonic response, i.e. the intensity of the electric field with double the frequency as the probe light, in a polymer diode with a dc electric field. The results presented here has been published in Ref [4].

6.3.1 Second Harmonic Generation

Before presenting the technique and the results, the second harmonic generation (SHG) will be introduced. SHG is the nonlinear optical effect which will be used

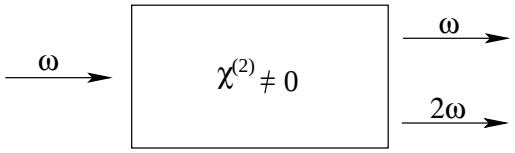

Fig. 6.2: The SHG process in a material with a non-zero second-order susceptibility.

to determine the built-in fields. The non-linear optical effects are often described by introducing the polarization P in the presence of the electric field $E(t)$. In linear optical effects there is a linear relationship between the polarization and the electric field, and proportionality is the linear susceptibility $\chi^{(1)}$:

$$P(\omega) = \varepsilon_0 \chi(\omega) E(\omega),$$

where ε_0 is the vacuum permittivity. In nonlinear optics terms besides the linear terms, that is terms which describes a nonlinear relationship between the polarization and the electric field, are included. This is done by introducing the polarization as a power series in the electric field:

$$P = \varepsilon_0 \chi^{(1)} E(\omega) + \varepsilon_0 \chi^{(2)} E^2(\omega) + \varepsilon_0 \chi^{(3)} E^3(\omega) + \cdots . \tag{6.4}$$

The proportionality constants $\chi^{(2)}$ and $\chi^{(3)}$ in (6.4) relating the polarization to the nonlinear terms of the electric field are the second- and third-order susceptibility, respectively. The polarization and electric fields are in general vectors and in case of anisotropic materials the susceptibility is a tensor. However, here it will be sufficient to treat them as scalars. The higher order susceptibilities are usually small quantities and very intense electric fields is therefore needed to observe the nonlinear phenomenons. As mentioned above one example of a nonlinear process is SHG where the light is generated at double the frequency of the incident light. The process can be considered a conversion of two photons with the frequency ω to one photon with the double frequency 2ω as illustrated in Fig. 6.2. SHG is often used to probe surfaces and interfaces because it is highly sensitive to broken symmetries such as surfaces and interfaces. The source of this sensitivity to broken symmetries is that in the dipole approximation, centrosymmetric materials can not generate a second harmonic (SH) signal making it possible to solely probe the surfaces and interfaces. Centrosymmetric materials have inversion symmetry and therefore a change of sign of the electric field must result in a change of sign of the polarization. Consider two situations with an electric field of E and $-E$. Due to the inversion symmetry the second order polarization will in the two situations be:

$$\begin{aligned} P^{(2)} &= \varepsilon_0 \chi^{(2)} E^2 && (6.5) \\ -P^{(2)} &= \varepsilon_0 \chi^{(2)} (-E)^2 \\ &= \varepsilon_0 \chi^{(2)} E^2. && (6.6) \end{aligned}$$

From these considerations it is evident that the second order polarization has to be zero for both (6.5) and (6.6) to be true. This only holds in the non-trivial case, i.e. with a non-zero electric field, if the second order susceptibility is zero.

In contrast to surfaces and interfaces, the bulk of a centrosymmetric material such as the randomly ordered molecules in a polymer, exhibit no SH signal. However, in the presence of a dc electric field it is possible to induce order in a material breaking the centrosymmetry making SHG possible. This technique is know as electric field induced second harmonic generation and is often abbreviated EFISHG or EFISH, the latter being the abbreviation used here. If the dc electric field is along the z-axis ($E_{dc,z}$) and the incident light has a component along the same axis ($E_z(\omega)$), the polarization can be describe by a third order susceptibility as:

$$P(2\omega) = \chi^{(3)} E_z(\omega) E_z(\omega) E_{dc,z},$$

as it was the case in electroabsorption measurements. This technique has previously been used on metal-oxide-semiconductor materials and poled polymers [106, 107, 108]. In these investigations the tightly focused probe beam was move along the applied electric dc field in order to successfully determine the distribution of the applied field.

6.3.2 EFISH in Polymer Light Emitting Diodes

EFISH has been applied to PLEDs in order to demonstrate the ability to use this tool to determine the diffusion voltage in PLED devices. EFISH was first applied to PLEDs by Hildebrandt *et al.*[109]. However, they only showed that it is possible to induce a SH signal with an electric field. It is shown here that SHG may actually be used to quantitatively characterize PLEDs. In PLEDs the situation is complicated by the constant background SH signal from the high work function electrode, ITO. The ITO is not centrosymmetric and therefore induces a SH signal. The SHG response from ITO on a glass substrate was investigated by Wang *et al.* and by measuring the SH signal dependence of the ITO thickness it was determined that the presence of SHG in ITO indeed is a bulk phenomenon. The SH signal was attributed a non-centrosymmetrical crystalline structure, and that the crystals had a preferred orientation making the SHG response dependent on the angle of incidence. However, by measurering a reference signal of the ITO alone and using this as input in the subsequent analysis of the EFISH measurement it is possible to determine the built-in voltage. The SH response of the polymer is described as a third order susceptibility $\chi_1 = \chi^{(3)}(-2\omega; \omega, \omega, 0)$, as mentioned above. The total SH intensity is then:

$$I(2\omega, V) \quad \propto \quad \left| \int_0^d \chi_1 E(\omega)^2 E_{eff}(z) dz + \chi_2 E(\omega)^2 \right|^2,$$

where d is the thickness of the polymer, $E(\omega)$ is the electric field of the incident light, $E_{eff}(z)$ is the static electric field corresponding to the effective voltage

$V_{eff} = V - V_{Bi}$, and the last term represents the constant SH signal from ITO having a second order susceptibility $\chi_2 = \chi^{(2)}$. The intensity of the SH signal can be calculated as:

$$\begin{aligned} I(2\omega, V) &\propto \left| \chi_1 E(\omega)^2 \int_0^d E_{eff}(z) dz + \chi_2 E(\omega)^2 \right|^2 \\ &\propto \left| \chi_1 E(\omega)^2 V_{eff} + \chi_2 E(\omega)^2 \right|^2 \\ &\propto \left| \chi_1 V_{eff} + \chi_2 \right|^2 I(\omega)^2 \\ &\propto \left| \chi_1 (V - V_{Bi}) + \chi_2 \right|^2 I(\omega)^2 \\ &\propto \left(|\chi_1|^2 (V - V_{Bi})^2 + |\chi_2|^2 + 2|\chi_1||\chi_2|(V - V_{Bi}) \cos\phi \right) I(\omega)^2 \end{aligned} \quad (6.7)$$

with ϕ being the phase difference between the two complex contributions to the SH signal, i.e. the EFISH and the ITO contribution.

From Eq. (6.7) it is observed that the SH signal is releated to the voltage through a second degree polynomial and that the last term in Eq. (6.7) is responsible for a shift of the minimum away from V_{Bi}. The fact that there are four unknowns (V_{Bi}, $|\chi_1|$, $|\chi_2|$, and ϕ) represents a problem since it is only possible determine three parameters from a fit of the experimental data to a second degree polynomial. Fortunately $|\chi_2|$ can be eliminated from the problem by measuring the constant background SH signal from ITO in an area without any low work function electrode to induce EFISH.

Although χ_1, χ_2, and ϕ have a wavelength dependence, the built-in voltage should be independent of the incident wavelength, because it only depends on the work functions of the contacts as described earlier. This will be demonstrated by using different probe beam wavelengths in the range from 740nm to 860nm. The findings will be compared with the electroabsorption measurements presented in Sec. 6.2 as well as differences in work functions for the electrodes.

The PLEDs were fabricated by spincoating MEH-PPV from a $6\frac{mg}{ml}$ solution on a $25 \times 25 mm^2$ ITO coated glass plate at 1000RPM. Before spinning, the ITO coated glass was cleaned by ultrasonication in acetone, demineralized water and ethanol and then blow dried. After spincoating of the polymer the metals were evaporated onto the sample starting with the calcium passing through a circular shadow mask with $6mm$ diameter followed by aluminum passing through a circular shadow mask with $15mm$ diameter, giving the device structure illustrated in Fig. 6.3. The metals were evaporated at a pressure of $\sim 10^{-6} mbar$ and with a $1\frac{nm}{s}$ deposition rate.

For the experiments a mode-locked, pulsed Ti-Sapphire laser with a $\sim 80 MHz$ repetition rate and $\sim 200 fs$ pulse duration was used. The experiments were performed with 60° angle of incidence and both polarizer and analyzer set to p-polarization. The experimental setup is illustrated in Fig. 6.4. The EFISH signal was detected with a photomultiplier tube attached to a monochromator. Both the externally applied voltage as well as the position on the sample along the

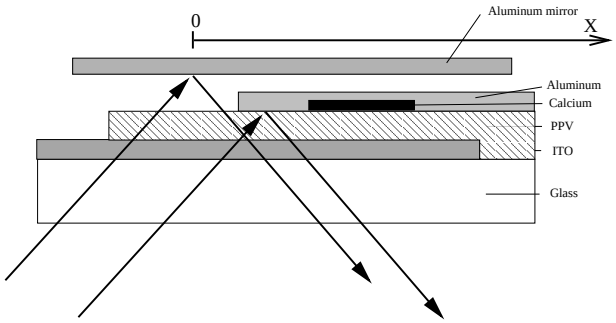

Fig. 6.3: Layer structure of PLEDs on a glass substrate. The figure also demonstrates how an aluminum mirror is mounted close to the sample for reference measurements.

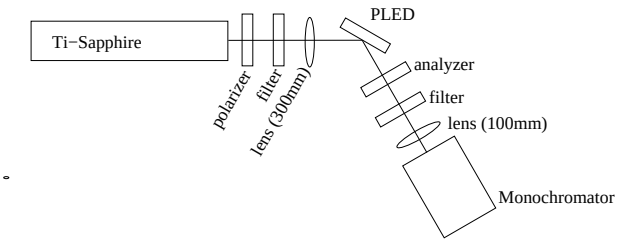

Fig. 6.4: The setup with 60^o angle of incidence . The first filter is to insure only light with the intended pump wavelength is incident onto the PLED and the second to remove reflected first harmonic beam. With polarizer and analyzer we choose the polarization of the pump and second harmonic beam, respectively.

x-axis indicated in Fig. 6.3 was scanned in the experiments. A monochromator was used to isolate the SH radiation appearing on a luminecense background. A filter absorbing light with wavelengths below $715nm$ was inserted before the device to remove any SH signal from laser or the optical components and a filter absorbing light with wavelengths above $475nm$ was inserted after the device to remove reflected light with the same wavelength as the probe beam.

A aluminum mirror was placed behind the PLED in an area not coated with metal electrodes. The purpose of this mirror was to measure the magnitude of the constant SH signal from the ITO in a situation close to the situation in a device, that is with a thin polymer film on top of the ITO, but without the metal electrode to induce a built-in electric field, which would produce a SH signal interfering with the SH signal of ITO. It is important to have the polymer on the ITO in the reference measurements because the polymer absorbs in the wavelength range of the SH light (370nm-430nm). Reference measurements with a different thickness of the polymer or with no polymer would therefore result in a false reference measurement. The aluminum mirror is positioned $\sim 1mm$

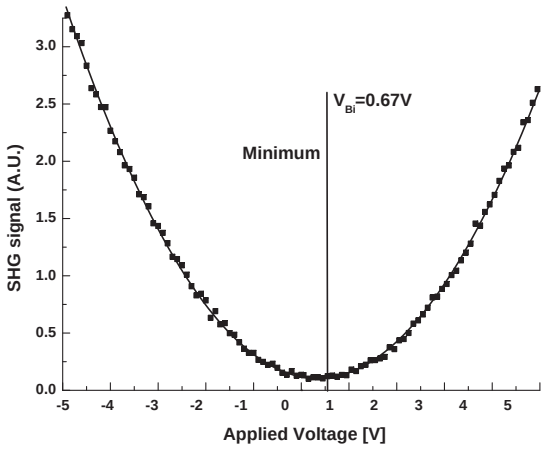

Fig. 6.5: EFISH voltage scan on a ITO/MEH-PPV/Al PLED where the squares are the measurements and the line is the best fit. Positive voltages indicate forward bias, that is, ITO biased positively. V_{Bi} is found to be 0.67V with a 0.998 coefficient of determination. Notice that V_{Bi} is shifted from the minimum of the polynomial as expected.

behind the PLED and therefore it is impossible to keep a tight focus on both the aluminum mirror and the metal contact in the PLED. Although it would be preferred to focus the laser tightly on the sample, since this would give the highest signal and therefore also the highest signal to noise ratio, this would result in a false reference measurement. For this reason the focal point was moved to approximately 5cm ahead of the PLED. At this distance there was a relatively small difference in intensitiesof the probe beam in the two situations and still high enough intensity to get good signal to noise ratio in EFISH measurements as illustrated in Fig. 6.5. This figure also illustrates that the EFISH signal indeed is related to the applied field through a second degree polynomial and confirming that (6.7) is true in both forward and reverse bias.

In each scan 100 measurements of the SH signal was performed at different voltages from $-5V$ to $5V$. These measurements were fitted to the second degree polynomial:

$$f(x) = ax^2 + bx + c, \tag{6.8}$$

with the least squares method. With $|\chi_2|$ determined by reference measurements as input it is possible to extract the three remaining quantities in (6.7) from the EFISH measurements. From the coefficients a, b, and c in (6.8) the quantities

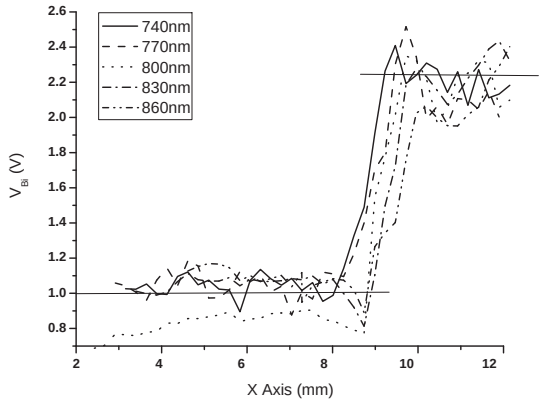

Fig. 6.6: Built-in voltages measured at different wavelengths and at different positions on the single layer PLED.

V_{Bi}, $|\chi_1|$, and ϕ from (6.7) can be determined by:

$$\begin{aligned} |\chi_1| &= \sqrt{a}, \\ V_{Bi} &= \frac{-b \pm \sqrt{b^2 - 4a(c - |\chi_2|^2)}}{2a}, \\ \phi &= \arccos\left(\frac{b + 2aV_{Bi}}{2\sqrt{a}|\chi_2|}\right). \end{aligned}$$

This is done at 60 positions along the x-axis with probe wavelengths: $740nm$, $770nm$, $800nm$, $830nm$, and $860nm$. The built-in voltages as function of position for the different wavelengths is plottet in Fig. 6.6. For all wavelengths and at all positions V_{Bi} have been determined from the coefficients of the second degree polynomial as described above, where the polynomials all have been fitted with a coefficient of determination (COD) no less than 0.99. From Fig. 6.6 V_{Bi} can estimated in the aluminum area to be $1.0eV$ and $2.25eV$ in the calcium area. Comparing this to the work function differences with ITO, aluminum and calcium have the following work functions: $\Phi_{ITO} = 5.2eV$, $\Phi_{Al} = 4.3eV$ and $\Phi_{Ca} = 2.9eV$ the measured built-in voltage matches the work function difference. The same conclusion was reached by Campbell *et al.*[104] using electroabsorption as mentioned in Sec. 6.2.

Similar measurements were performed on a device with MEH-PPV sandwiched between a ITO/PEDOT:PSS cathode and a Al anode. The ITO coated glass was cleaned with the same procedure as described previously. The PEDOT:PSS was subsequently spincoated from a 0.7% solution at $1000RPM$ and

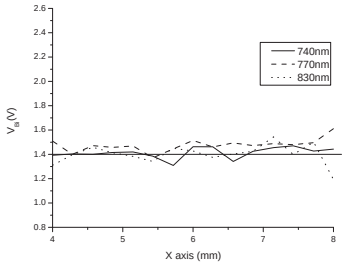

Fig. 6.7: Built-in voltages measured at different wavelengths and at different positions on the double layer PLED with PEDOT:PSS as hole injecting layer.

afterwards the sample was heated to 130°C for 30min to remove any remaining solvent. The rest of the device fabrication, i.e. spincoating of polymer and cathode evaporation, was performed as described previously. The measurements were performed with three different probe beam wavelengths: $740nm$, $770nm$, and $830nm$ and analyzed afterwards. The results of the analysis are illustrated in Fig. 6.7. From Fig. 6.7 it is observed that the built-in voltages is at all wavelengths $1.4V$, that is an increase of $0.4V$ compared to the device without PEDOT:PSS. A similar increase in the built-in voltage upon addition of PEDOT:PSS was was measured by Brown *et al.* using electroabsorption[101].

This means the technique used to determine internal electric fields in metal-semiconductor and metal-oxide-semiconductor interfaces also can be applied to determine built-in voltages in organic semiconductors, even organic semiconductors with a constant background SH signal.

6.4 Conclusion

In this chapter second harmonic generation and electric field induced second harmonic generation was introduced, and the latter has been developed as a non-destructive *in situ* tool to measure the built-in voltage in PLEDs. The situation is complicated by the constant second harmonic signal originating from the non-centrosymmetric ITO electrode. The measurement showed excellent agreement with the predicted dependence between the second harmonic signal and the squared applied voltage. From these measurements the built-in voltage was determined with different probe beam wavelengths and with different contact electrodes using the second harmonic reference measurement of MEH-PPV on ITO as input. The built-in voltages found to match the differences in work function in a device with both ITO/MEH-PPV/Al and ITO/MEH-PPV/Ca layered

structure. The built-in voltage also matched the work function difference in a double layer device with a ITO/PEDOT:PSS/MEH-PPV/Al layer structure. In doing it was also demonstrated that it is possible to extract information from EFISH measurements with a constant background SH signal, in this case from the high work function electrode, ITO.

Part IV

Concluding Remarks

Summary of Conclusions

In Part I organic light emitting diodes was introduced along with results describing the major influences on device operation in general and efficiency in particular. Also included was results from a theoretical modeling of conjugated porphyrin polymers using the Density Functional-based Tight-Binding approach. The calculations showed that porphyrin polymers have an optical gap in the IR range and a small exciton binding energy making them candidates for solar cells absorbing in the IR range. The study also showed that the exciton binding energy is particularly small in metal containing porphyrin polymers.

In Chap. 4 a number of different conjugated polymers spanning the entire visible range was characterized. The first group of polymers investigated was the red and green emitting PPV-derivatives ranging from the commercially available MEH-PPV to the green emitting copolymers based on PPV and phenanthroline synthesized by the Chemistry Department at Aalborg University. The second group of polymers was the blue emitting polyfluorenes. Emission from these polymers was blue-shifted by incorporating a conjugation breaking binaphthyl monomer in a polyfluorene copolymer. Green emission was observed in devices with no hole injecting layer. The green emission was attributed emission from fluorenone defects, that is, oxidation defects. The oxidation did not occur in devices with a hole injecting layer, because this layer protected the polymer from oxidation by the ITO electrode. The third group of polymers was phenylene based copolymers. These polymers show a clear difference between EL and PL, which was attributed stronger electron-phonon coupling and excimers in EL, which was not present in PL. The stronger electron-phonon coupling in EL was due to the difference in recombination zone. In EL the recombination zone is near the metal/polymer interface whereas recombination is evenly distributed in PL. In Chap. 5 red emission was further investigated due to its use in polymer based displays. Red emission in such devices is particularly difficult because of the broad emission from polymers due to vibrational states and inhomogeneous

broadening and the low sensitivity of the eye towards red emission, making most red emitters appear orange. The problem was approached by blending a Eu complex having emission at $613nm$ and very sharp emission peak into a blue emitting polymer. Pure red emission was, however, difficult to achieve because of the small spectral overlap between emission from the polymer and absorption of the Eu complex.

In Chap 6 a new technique for determining the built-in field in device was devoloped. The source of the built-in field is the difference in workfunctions in contact materials. Electric field induced second harmonic generation measurements was performed on a device and the built-in field could be extracted from these measurements in different combinations of contact materials.

Outlook

The field of polymer light emitting diodes has come a long way since it beginning in the early 1990's but there is still plenty of room for improvements in developing efficient devices with emission in the entire visible range plus the IR and the UV range. By doping the polymer with erbium complexes it is possible to achieve emission at $1.54\mu m$, i.e. the optical communications wavelength, making optical communication devices based on polymers possible. Further investigations with EFISH on other contact materials and with other polymers would certainly also be interesting because the contact materials have great influence on device operation and efficiency. The EFISH method could also be applied to devices with other contact materials and polymers than presented here. The latter is particular interesting since the choice of polymer should have no influence on the results, thus it could be used to verify the method.

Bibliography

Bibliography

[1] T. G. Pedersen, T. B. Lynge, P. K. Kristensen, and P. M. Johansen. Theoretical study of conjugated porphyrin polymers. *Thin Solid Films*, **477**:182, (2005).

[2] P. K. Kristensen, T. G. Pedersen, K. Zhu, and D. Yu. Energy transfer from polyfluorene based polymers to europium complex. *Eur. Phys. J. Appl. Phys.*, **37**:57, (2007).

[3] D. Yu, K. Zhu, P.K. Kristensen, T. Garm Pedersen, and R. Wimmer Poly(p-phenylenevinylene) derivatives containing electron-transporting 1,10-phenanthroline segments. *Polymer Preprints*, **48**;105, (2008).

[4] P. K. Kristensen, J. Rafaelsen, T. G. Pedersen, and K. Pedersen. Diffusion voltage in polymer light emitting diodes measured with electric field induced second harmonic generation. *Phys. Stat. Sol. (c)*, 2:3993, (2005).

[5] M. Pope, H. P. Kallmann, and P. Magnante. Electroluminescence in organic crystals. *J. Chem. Phys.*, **38**:2042, (1963).

[6] C. W. Tang and S. A. VanSlyke. Organic electroluminescent diodes. *Appl. Phys. Lett*, **51**:913, (1987).

[7] C. W. Tang, S. A. VanSlyke, and C. H. Chen. Electroluminescence in doped organic thin films. *J. Appl. Phys.*, **85**:3610, (1989).

[8] R. Ballardini, G. Varani, M. T. Indelli, and F. Scandola. Phosphorescent 8-quinolinol metal chelates. excited-state properties and redox behavior. *Inorg. Chem.*, **25**:3858, (1986).

[9] S. A. VanSlyke, P. S. Bryan, and F. V. Lovecchio. U.s. patent 5,150,006 (1990).

[10] T. D. Eck, E. L. Weary, and D. M. Hercules. Some chelates of 4-hydroxy-1,5-naphthyridine. *J. Inorg. Nucl. Chem.*, **28**:2439, (1966).

[11] C. H. Chen and J. Shi. Metal chelates as emitting materials for organic electroluminescence. *Coord. Chem. Rev.*, **171**:161, (1998).

[12] W. P. Su, J. R. Schrieffer, and A. J. Heeger. Solitons in polyacetylene. *Phys. Rev. Lett.*, **42**:1698, (1979).

[13] D. Porezag, Th. Frauenheim, Th. Köhler, G. Seifert, and R. Kaschner. Construction of tight-binding-like potentials on the basis of density-functional theory: Application to carbon. *Phys. Rev. B*, **51**:12947, (1995).

[14] T. B. Lynge. *Tight-Binding Treatment of Conjugated Polymers*. PhD thesis, Aalborg University, (2004).

[15] A. Tsuda and A. Osuka. Fully conjugated porphyrin tapes with electronic absorption bands that reach into infrared. *Science*, **293**:79, (2001).

[16] J. H. Burroughes, D. D. C. Bradley, A. R. Brown, R. N. Marks, K. Mackey, R. H. Friend, P. L. Burn, and A. B. Holmes. Light-emitting diodes based on conjugated polymers. *Nature (London)*, **347**:539, (1990).

[17] G. Mao, J. E. Fischer, F. E. Karasz, and M. J. Winokur. Nonplanarity and ring torsion in poly(p-phenylene vinylene). a neutron-diffraction study. *J. Chem. Phys.*, **98**:712, (1993).

[18] R. A. Wessling and R. G. Zimmerman. U.s. patent 3401152 (1968) and u.s. patent 3406677 (1972).

[19] R. W. Lenz, C.-C. Han, J. Stenger-Smith, and F. E. Karasz. Preparation of poly(phenylene vinylene) from cycloalkylene sulfonium salt monomers and polymers. *J. Polym. Sci. A.*, **26**:3241, (1988).

[20] S. H. Askari, S. D. Rughooputh, F. Wudl, and A. J. Heeger. Soluble conducting polymers: Dhppv. *Polym. Preprints*, **30**:157, (1989).

[21] D. Braun and A. J. Heeger. Visible light emission from semiconducting polymer diodes. *Appl. Phys. Lett.*, **58**:1982, (1991).

[22] L. Lauchlan, S. Etemad, T.-C. Chung, A. J. Heeger, and A. G. MacDiarmid. Photoexcitations in polyacetylene. *Phys. Rev. B.*, **24**:3701, (1981).

[23] P. Gomes da Costa and E. M. Conwell. Excitons and the band gap in poly(phenylene vinylene). *Phys. Rev. B.*, **48**:1993, (1993).

[24] U. Rauscher, H. Bässler, D. D. C. Bradley, and M. Hennecke. Exciton versus band description of the absorption and luminescence spectra in poly(p-phenylenevinylene). *Phys. Rev. B.*, **42**:9830, (1990).

[25] D. Beljonne, Z Shuai, R. H. Friend, and J. L. Brédas. Theoretical investigation of the lowest singlet and triplet states in poly(paraphenylene vinylene)oligomers. *J. Chem. Phys.*, **102**:2042, (1995).

[26] Th. Förster. Zwischenmolekulare energiewanderung und fluoreszenz. *Ann. der Phys.*, **2**:55, (1948).

[27] M. Pope and C. E. Swenberg. *Electronic Processes in Organic Crystals.* Oxford, New York, (1982).

[28] D. L. Dexter. A theory of sensitized luminescence in solids. *J. Chem. Phys.*, **21**:836, (1952).

[29] Y.-Y. Noh, C.-L. Lee, and J.-J. Kim. Energy transfer and device performance in phosphorescent dye doped polymer light emitting diodes. *J. Chem. Phys.*, **118**:2853, (2003).

[30] F.-C. Chen, S.-C. Chang, G. He, S. Pyo, Y. Yang, M. Kurotaki, and J. Kido. Energy transfer and triplet exciton confinement in polymeric electrophosphorescent devices. *J. Polym. Sci. B.*, **41**:2681, (2003).

[31] M. Yan, L. J. Rothberg, F. Papadimitrakopoulos, M. E. Galvin, and T. M. Miller. Defect quenching of conjugated polymer luminescence. *Phys. Rev. Lett.*, **73**:744, (1994).

[32] J. Bigerson, M. Fahlman, P. Bröms, and W. R. Salaneck. Conjugated polymer surfaces and interfaces: a mini-review and some new results. *Synth. Met.*, **80**:125, (1996).

[33] G. G. Malliaras and J. C. Scott. The roles of injection and mobility in organic light emitting diodes. *J. Appl. Phys.*, **83**:5399, (1997).

[34] P. W. M. Blom, M. J. M. de Jong, and J. J. M. Vleggaer. Electron and hole transport in poly(p-phenylene vinylene) devices. *Appl. Phys. Lett.*, **68**:3308, (1996).

[35] Y.-S. Chen and H.-F. Meng. Intrachain carrier transport in conjugated polymer with structural and chemical defects. *Phys. Rev. B*, **66**:035202, (2002).

[36] G. G. Malliaras and J. C. Scot. Numerical simulations of the electrical characteristics and the efficiencies of single-layer organic light emitting diodes. *J. Appl. Phys*, **85**:7426, (1999).

[37] P. W. M. Blom, M. J. M. de Jong, and M. G. van Munster. Electric-field and temperature dependence of the hole mobility in poly(p-phenylene vinylene. *Phys. Rev. B*, **55**:656, (1997).

[38] J.-S. Kim, P. K. H. Ho, N. C. Greenham, and R. H. Friend. Electroluminescence emission pattern of organic light-emitting diodes: Implications for device efficiency calculations. *J. Appl. Phys.*, **88**:1073, (2000).

[39] Y. Cao, I. D. Parker, G. Yu, C. Zhang, and A. J. Heeger. Improved quantum efficiency for electroluminescence in semiconducting polymers. *Nature*, **397**:414, (1999).

[40] G. Cnossen, K. E. Drabe, and D. A. Wiersma. Fluorescence properties of submonolayers of rhodamine 6g in front of a mirror. *J. Chem. Phys.*, **98**:5276, (1993).

[41] A. Kawski, E. Kuteń, and J. Kamiński. Fluorescence quenching and nonradiative energy transfer in solutions. *J. Phys. B*, **6**:1907, (1973).

[42] P. W. M. Blom, M. C. J. M. Vissenberg, J. N. Huiberts, H. C. F. Martens, and H. F. M. Schoo. Optimum charge-carrier mobility for a polymer light-emitting diode. *Appl. Phys. Lett.*, **77**:2057, (2000).

[43] L. C. Lin, H. F. Meng, J. T. Shy, S. F. Hong, L. S. Yu, C. H. Chen, H. H. Liaw, C. C. Huang, K. Y. Peng, and S. A. Chen. Triplet-to-singlet exciton formation in poly(p-phenylene-vinylene) light-emitting-diodes. *Phys. Rev. Lett.*, **90**:036601, (2003).

[44] H. Becker, S. E. Burns, and R. H. Friend. Effect of metal films on the photoluminescence and electroluminescence of conjugated polymers. *Phys. Rev. B*, **56**:1893, (1997).

[45] Z. Shuai, D. Beljonne, R. J. Silbey, and J. L. Brédas. Singlet to triplet exciton formation rates in conjugated polymer light-emitting diode. *Phys. Rev. Lett.*, **84**:131, (2000.

[46] M. Wohlgenannt, K. Tandon, S. Mazumdar, S. Ramasesha, and Z. V. Vardeny. Formation cross-sections of singlet and triplet excitons in π-conjugated polymers. *Nature*, **409**:494, (2001).

[47] J. S. Wilson, A. S. Dhoot, A. J. A. B. Seeley, M. S. Khan, A. Köhler, and R. H. Friend. Spin-dependent exciton formation in π-conjugated compounds. *Nature*, **413**:828, (2001).

[48] N. C. Greenham, I. D. W. Samuel, G. R. Hayes, R. T. Phillips, Y. A. R. R. Kessener, S. C. Moratti, A. B. Holmes, and R. H. Friend. Measurement of absolute photoluminescence quantum efficiencies in conjugated polymers. *Chem. Phys. Lett.*, **241**:89, (1995).

[49] N. T. Harrison, G. R. Hayes, R. T. Phillips, and R. H. Friend. Singlet intrachain exciton generation and decay in poly(p-phenylenevinylene). *Phys. Rev. Lett.*, **77**:1881, (1996).

[50] J. J. M. Halls, K. Pichler, R. H. Friend, S. C. Moratti, and A. B. Holmes. Exciton diffusion and dissociation in a poly(p-phenylenevinylene)/c_{60} heterojunction photovoltaic cell. *Appl. Phys. Lett.*, **68**:3120, (1996).

[51] H. F. Wittmann, R. H. Friend, M. S. Khan, and J. Lewis. Optical spectroscopy of platinum and palladium containing poly-ynes. *J. Chem. Phys.*, **101**:2693, (1994).

[52] M. A. Baldo, D. F. Brien, M. E. Thompson, and S. R. Forres. Excitonic singlet-triplet ratio in a semiconducting organic thin film. *Phys. Rev. B*, **60**:14422, (1999).

[53] G. Gustafsson, Y. Cao, G. M. Treacy, F. Klavetter, N. Colaneri, and A. J. Heeger. Flexible light-emitting diodes made from soluble conducting polymers. *Nature*, **357**:477, (1992).

[54] Y. Yang and A. J. Heeger. Polyaniline as a transport electrode for polymer light-emitting diodes: Lower operation voltage and higher efficiency. *Appl. Phys. Lett.*, **64**:1245, (1994).

[55] Y. Cao, G. M. Treacy, P. Smith, and A. J. Heeger. Solution-cast films of polyaniline: Optical-quality transparent electrodes. *Appl. Phys. Lett.*, **60**:2711, (1992).

[56] S. A. Carter, M. Angelopoulos, S. Karg, P. J. Brock, and J. C. Scott. Polymeric anodes for improved polymer light-emitting diode performance. *Appl. Phys. Lett.*, **70**:2067, (1997).

[57] S. Karg, J. C. Scott, J. R. Salem, and M. Angelopoulos. Increased brightness and lifetime of polymer light-emitting diodes with polyaniline anodes. *Synth. Met.*, **80**:111, (1996).

[58] J. C. Scott, J. H. Kaufman, P. J. Brock, R. DiPietro, J. Salem, and J. A. Goitia. Degradation and failure of meh-ppv light-emitting diodes. *J. Appl. Phys.*, **79**:2745, (1996).

[59] A. Berntsen, Y. Croonen, C. Liedenbaum, H. Schoo, R.-J. Visser, J. Vleggaar, and P. van de Weijer. Stability of polymer leds. *Opt. Mater.*, **9**:125, (1998).

[60] P. C. Jukes, S. J. Martin, A. M. Higgins, M. Ceoghegan, R. A. L. Jones, S. Langridge, A. Wehrum, and S. Kirchmeyer. Controlling the surface composition of poly(3,4-ethylene dioxythiophene)-poly(styrene sulfonate) blends by heat treatment. *Adv. Mater.*, **16**:807, (2004).

[61] G. Greczynski, Th. Kugler, and W. R. Salaneck. Characterization of the pedot-pss system by means of x-ray and ultraviolet photoelectron spectroscopy. *Thin Solid Films*, **354**:129, (1999).

[62] T. W. Hagler, K. Pakbar, K. F. Voss, and A. J. Heeger. Enhanced order and electronic delocalization in conjugated polymers oriented by gel processing in polyethylene. *Phys. Rev. B*, **44**:8652, (1991).

[63] M. Liess, S. Jeglinski, Z. V. Vardeny, M. Ozaki, K. Yoshino, Y. Ding, and T. Barton. Electroabsorption spectroscopy of luminescent and nonluminescent π-conjugated polymers. *Phys. Rev. B*, **56**:15712, (1997).

[64] S. Karabunarliev, E. R. Bittner, and M. Baumgarten. Franck-condon spectra and electro-libration coupling in para-phenyls. *J. Chem. Phys.*, **114**:5863, (2001).

[65] S. C. Moratti, D. D. C. Bradley, R. Cervini, R. H. Friend, N. C. Greenham, and A. B. Holmes. Light-emitting polymer leds. *SPIE*, **2144**:108, (1994).

[66] A. B. Holmes, A. Kraft, and A. C. Grimsdale. Electroluminescent conjugated polymers - seeing polymers in a new light. *Angew. Chem. Int. Ed.*, **37**:402, (1998).

[67] K. S. Wong, T. Sun, X.-L. Liu, J. Pei, and W. Huang. Optical properties and time-resolved photoluminescence of conjugated polymers with europium complex side chain as an emitter. *Thin Solid Films*, **417**:85, (2002).

[68] Q. Pei and Y. Yang. Efficient photoluminescence and electroluminescence from a soluble polyfluorene. *J. Am. Chem. Soc.*, **118**:7416, (1996).

[69] A. W. Grice, D. D. C. Bradley, M. T. Bernius, M. Inbasekaran, W. W. Wu, and E. P. Woo. High brightness and efficiency blue light-emitting polymer diodes. *Appl. Phys. Lett.*, **73**:629, (1998).

[70] A. J. Campbell, D. D. C. Bradley, and H. Antoniadis. Quantifying the efficiency of electrodes for positive carrier injection into poly(9,9-dioctylfluorene) and representative copolymers. *J. Appl. Phys.*, **89**:3343, (2001).

[71] X. Jiang, S. Liu, H. Ma, and A. K.-Y. Jen. High-performance blue light-emitting diode based on a binaphthyl-containing polyfluorene. *Appl. Phys. Lett.*, **76**:1813, (2000).

[72] L. Zheng, R. C. Urian, Y. Liu, A. K.-Y. Jen, and L. Pu. A binaphthyl-based conjugated polymer for light-emitting diodes. *Chem. Mater.*, **12**:13, (2000).

[73] R. B. Capaz and M. J. Caldas. *Ab initio* calculations of structural and dynamical properties of poly(p-phenylene) and poly(p-phenylene vinylene). *Phys. Rev. B*, **67**:205205, (2003).

[74] U. Scherf and E. J. W. List. Semiconducting polyfluorenes - towards reliable structure-property relationships. *Adv. Mater.*, **14**:477, (2002).

[75] A. P. Kulkarni, X. Kong, and S. A. Jenekhe. Fluorenone-containing polyfluorenes and oligofluorenes: Photophysics, origin of the green emission and efficient green electroluminescence. *J. Phys. Chem.*, **108**:8689, (2004).

[76] W.-L. Yu, J. Pei, W. Huang, and A. J. Heeger. Spiro-functionalized polyfluorene derivatives as blue light-emitting materials. *Adv. Mater.*, **12**:828, (2000).

[77] J. Peng, B.-Y. Yu, C.-H. Pyun, C.-H. Kim, and J.-I. Jin. The effect of a metal electrode on ppv electroluminescence processes. *J. Lumin.*, **75**:361, (1997).

[78] B. Hu and F. E. Karasz. Interfacial effects in polymer leds. *Chem. Phys.*, **227**:263, (1998).

[79] Z. Lin, S. Priyadarshy, A. Bartko, and D. H. Waldeck. Photophysics and intramolecular excimer formation in a constrained anthracenyl diadduct. *J. Photochem. Photobiol., A*, **110**:131, (1997).

[80] J. F. Deus, M. L. Andrade, T. D. Z. Atvars, and L. Akcelrud. Photo and electroluminescence studies of poly(methyl methacrylate-co-9-anthryl methyl methacrylate). *Chem. Phys.*, **297**:177, (2004).

[81] K. Kaeriyama, Y. Tsukahara, S. Negoro, N. Tanigaki, and H. Masuda. Preparation and properties of soluble polyphenylenes. *Synth. Met.*, **84**:263, (1997).

[82] Y. Kim, S. Kwon, D. Yoo, M. F. Rubner, and M. S. Wrighton. A novel, bright blue electroluminescent polymer: A diphenylanthracene derivative. *Chem. Mater.*, **9**:2699, (1997).

[83] Q. Sun, H. Wang, C. Yang, G. He, and Y. Li. Blue-green light-emission lecs based on block copolymers containing di(α-naphthalene vinylene)benzene chromophores and tri(ethylene oxide) spacers. *Synth. Met.*, **128**:161, (2002).

[84] H.-K. Shim, T. Ahn, and S.-Y. Song. Synthesis and led device properties of carbazole and naphthalene contained conjugated polymers. *Thin Solid Films*, **417**:7, (2002).

[85] A. K.-Y. Jen, U. Liu, Q.-S. Hu, and L. Pu. Efficient light-emitting diodes based on a binaphthyl-containing polymer. *Appl. Phys. Lett.*, **75**:3745, (1999).

[86] J. Lee, N. S. Cho, J. Lee, S. K. Lee, and K.-K. Shim. Emission color tuning of new fluorene-based alternating copolymers containing low band gap dyes. *Synth. Met.*, **155**:73, (2005).

[87] E. I. Mal'tsev, D. A. Lypenko, B. I. Shapiro, M. A. Brusentseva, G. H. W. Milburn, J. Wright, A. Hendriksen, V. I. Berendyaev, B. V. Kotov, and A. V. Vannikov. Electroluminescence of polymer/j-aggregate composites. *Appl. Phys. Lett.*, **75**:1896, (1999).

[88] L. R. Melby, N. J. Rose, E. Abramson, and J. C. Caris. Synthesis and fluorescence of some trivalent lanthanide complexes. *J. Am. Chem. Soc.*, **86**:5117, (1964).

[89] G. A. Crosby, R. E. Whan, and R. M. Alire. Intramolecular energy transfer in rare earth chelates. role of the triplet state. *J. Chem. Phys.*, **34**:743, (1961).

[90] M. D. McGehee, T. Bergstedt, C. Zhang, A. P. Saab, M. B. O'Regan, G. C. Bazan, V. I. Srdanov, and A. J. Heeger. Narrow bandwidth luminescence from blends with energy transfer from semiconducting conjugated polymers to europium complexes. *Adv. Mater.*, **11**:1349, (1999).

[91] H. Nabika and S. Deki. Surface-enhanced luminescence from Eu^{3+} complex nearby ag colloids. *Eur. Phys. J. D*, **24**:369, (2003).

[92] A. Beeby, L. M. Bushby, D. Maffeo, and J. A. G. Williams. The efficient intramolecular sensitisation of terbium (iii) and europium(iii) by benzophenone-containing ligands. *J. Chem. Soc., Perkin Trans.*, page 1281, (2000).

[93] R. G. Sun, Y. Z Wang, Q. B. Zheng, H. J. Zhang, and A. J. Epstein. $1.54\mu m$ infrared photoluminescence and electroluminescence from an erbium organic compound. *J. Appl. Phys.*, **87**:7589, (2000).

[94] J. Kido, H. Hayase, K. Hongawa, K. Nagai, and K. Okuyama. Bright red light-emitting organic electroluminescent devices having a europium complex as an emitter. *Appl. Phys. Lett.*, **65**:2124, (1994).

[95] L. Liu, W. Li, Z. Hong, J. Peng, X. Liu, C. Liang, Z. Liu, J. Yu, and D. Zhao. Europium complexes as emitters in organic electroluminescent devices. *Synth. Met.*, **91**:267, (1997).

[96] J. Pei, X. Liu, W. Yu, Y. Lai, Y. Niu, and Y. Cao. Efficient energy transfer to achieve narrow bandwidth red emission from eu^{3+}-grafting conjugated polymers. *Macromolecules*, **35**:7274, (2002).

[97] Q. Ling, M. Yang, W. Zhang, H. Lin, G. Yu, and F. Bai. Pl and el properties of a novel eu-containing copolymer. *Thin Solid Films*, **417**:127, (2002).

[98] Z. Wang and I. D. W. Samuel. Energy transfer from a polymer host to a europium complex in light-emitting diodes. *J. Lumin.*, **111**:199, (2005).

[99] C. Adachi, M. A. Baldo, and S. R. Forrest. Electroluminescence in organic light emitting devices employing a europium chelate doped in a wide energy gap bipolar conducting host. *J. Appl. Phys.*, **87**:8049, (2000).

[100] M. H. V. Werts, M. A. Duin, J. W. Hofstraat, and J. W. Verhoeven. Bathochromicity of michler's ketone upon coordination with lanthanide(iii) β-diketonates enables efficient sensitisation eu^{3+} for luminescence under visible light excitation. *Chem. Commun.*, **9**:799, (1999).

[101] T. M. Brown, J. S. Kim, R. H. Friend, F. Cacialli, R. Daik, and W. J. Feast. Effect of poly(3,4ethylene dioxythiophene) on the built-in field in polymer light-emitting diodes probed by electroabsorption spectroscopy. *Synth. Met.*, **111**:285, (2000).

[102] T. M. Brown, J. S. Kim, R. H. Friend, F. Cacialli, R. Daik, and W. J. Feast. Built-in field electroabsorption spectroscopy of polymer light-emitting diodes incorporating a doped poly(3,4-ethylene dioxythiophene) hole injection layer. *Appl. Phys. Lett.*, **75**:1679, (1999).

[103] I. H. Campbell, J. D. Ferraris, T. W. Hagler, M. D. Joswick, I. D. Parker, and D. L. Smith. Measuring internal electric fields in organic light-emitting diodes using electroabsorption spectroscopy. *Polym. Adv. Technol.*, **8**:417, (1997).

[104] I. H. Campbell, T. W. Hagler, D. L. Smith, and J. P. Ferraris. Direct measurement of conjugated polymer electronic excitation energies using metal/polymer/metal structures. *Phys. Rev. Lett.*, **76**:1900, (1996).

[105] X. Wei, S. A. Jeglinski, and Z. V. Vardeny. Photoresponse and electroresponse studies of polymer light-emitting diodes. *Synth. Met.*, **85**:1215, (1997).

[106] G. Lüpke, C. Meyer, C. Ohlhoff, H. Kurz, S. Lehmann, and G. Marowsky. Optical second-harmonic generation as a probe of electric-field-induced perturbation of centrosymmetric media. *Opt. Lett.*, **20**:1997, (1995).

[107] O. A. Aktsipetrov, A. A. Fedyanin, E. D. Mishina, A. N. Rubtsov, C. W. van Hasselt, M. A. C. Devillers, and Th. Rasing. dc-electric-field-induced second-harmonic generation in si(111)-sio_2-cr metal-oxide-semiconductor structures. *Phys. Rev. B*, **54**:1825, (1996).

[108] C. Ohlhoff, G. Lüpke, C. Meyer, and H. Kurz. Static and high-frequency electric fields in silicon mos and ms structures probed by optical second-harmonic generation. *Phys. Rev. B*, **55**:4596, (1997).

[109] R. Hildebrandt, H. Keller, G. Marowsky, W. Brtting, T. Fehn, M. Schwoerer, and J.E. Sipe. Electric-field-induced optical second-harmonic generation in poly(phenylene vinylene) light-emitting diodes. *Chem. Phys.*, **245**:341, (1999).

Dansk resume

Denne ph.d.-afhandling behandler lys emitterende dioder baseret på konjugerede polymerer. Der er flere grunde til at polymer baserede lys dioder er interessante. Blandt disse er produktionen af lys dioder baseret på polymerer er let, hvor polymeren blot spin coates på et ledende materiale som skal virke som den ene kontakt og efterfølgende påføres den anden kontakt og produktionen er afsluttet. Kontakterne kan være fleksible og det er således muligt at lave et fleksibelt display. Endelig er det muligt at designe farvesammenstningen af lyset fra polymeren, ved at ændre på den kemiske struktur af polymeren.

I denne afhandling undersøges en række polymere for lys udsendelse fra polymer baserede lys emitterende dioder. De undersøgte polymere kan deles op i tre grupper, phenylene vinylene afledte polymere som udsender rødt og grønt lys, polyfluorene afledte som udsender blåt lys og phenylene baserede copolymere som udsender blåt og grønt lys. Endelig er det beskrevet hvorledes tilføjelse af et Eu komplex til en blå emitterende polymer kan benyttes til at få rødt lys med skarpe toppe, praktisk til udsendelse af rød lys i en polymer baseret display.

Den sidste del omhandler undersøgelser af kontakt materialer i polymer baserede dioder. Denne undersøgelse af kontakterne er vigtigt da valget af kontakt har stor indflydelse på effektiviteten, da de bestemmer let ladninger er injekteret i polymeren. Til undersøgelsen af kontakt materialerne er der udviklet en *in situ*, ikke-destruktiv målemetode baseret på optisk anden harmonisk generation.